ON THE DISTRIBUTIONS OF LOW-ENERGY PROTONS AND ELECTRONS IN THE EARTH'S MAGNETOSPHERE*

by

L. A. Frank

September 1967

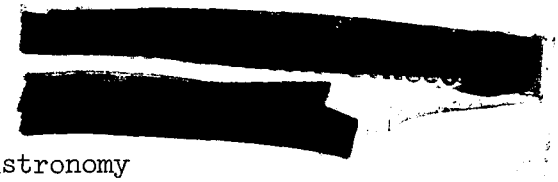

Department of Physics and Astronomy
University of Iowa
Iowa City, Iowa

*This research was supported in part by the National Aeronautics and Space Administration under Grant NsG-233-62 and Contract NAS5-2054 and by the Office of Naval Research under Contract Nonr-1509(06). Presented at the Advanced Study Institute, Earth's Particles and Fields, Stadt Freising, Germany, 31 July - 11 August, 1967.

Introduction

The following brief introductory comments serve as an abridged summary of the status of low-energy charged particle observations within the earth's magnetosphere during 1965 as presented at the first Advanced Study Institute on the geomagnetically trapped radiation [McCormac, 1966] and provide a framework for the present discussions of the complex spatial distributions and temporal variations of low-energy proton and electron intensities which have recently been detected and initially surveyed within the earth's radiation zones and their environs. The study of low-energy charged particle intensities over geocentric radial distances ~ 1 to 10 R_E (R_E, earth radius) has progressed slowly when compared to the rapidly increasing knowledge concerning higher energy proton ($E \gtrsim 100$ keV) and electron ($E \gtrsim 50$ keV) distributions due to severe obstacles in constructing observational apparatus with sufficient sensitivity, energy thresholds and immunities to background responses attributable to the energetic, penetrating charged particles of the inner and outer radiation zones and to solar ultraviolet emissions. By 1965 exploratory searches for large intensities of low-energy protons and electrons with satellite-borne retarding potential analyzers, plasma cups and CdS crystals had identified several regions within and near the magnetosphere in the

vicinity of the magnetic equatorial plane which were characterized by relatively high charged particle intensities. Two of these regions are evident in the summary of initial observations which is presented in Figure 1 [Frank, 1966a]; viz., (1) within the magnetosheath which lies between the magnetospheric boundary (magnetopause) and the transition shock and (2) in the dark hemisphere of the magnetosphere at geocentric radial distances exceeding $\sim 8\ R_E$ near the magnetic equatorial plane (see Frank [1966a] for the appropriate references for the several measurements displayed in Figure 1 and the following Figure 2). Of primary interest during the course of our present survey is the evening hemisphere of the magnetosphere over geocentric radial distances ~ 1 to $15\ R_E$. The strong dependence of the spatial distributions of electron intensities upon electron energy is demonstrated by a comparison of the spatial distributions of electron ($E \sim 50$ keV) intensities shown in Figure 2 [Frank, 1966a] with the summary of lower energy electrons (~ 1 keV) of the previous Figure 1. The complexity of the electron distributions in the outer radiation zone is further stressed by the comprehensive study of the temporal variations of higher energy electron intensities presented in Figure 3 [Owens and Frank, 1967] which displays iso-intensity contours for omnidirectional intensities of electrons ($E \geq 40$ keV, ≥ 230 keV and ≥ 1.6 MeV) as functions of shell parameter L and time at the geomagnetic equator during the period October through November 1962.

Our eventual understanding of these distributions of charged particles and their temporal variations in intensities, presumably originating via a presently unknown 'local acceleration' mechanism in the earth's magnetosphere with the flow of solar plasma as the primal energy source, depends heavily upon detailed observations of lower energy charged particles with energies ~ 1 eV to tens of keV, as well as of geomagnetic and geoelectric fields. Several recent observations of proton and electron intensities over the energy range extending from ~ 100 eV to 50 keV which are directly pertinent toward delineating several gross features of the dynamics of the earth's magnetosphere are summarized in the following discussion.

Brief Description of Instrumentation and Orbit

As a major fraction of the observations of low-energy charged particle intensities in the outer radiation zone summarized herein was obtained with an array of electrostatic analyzers borne on the earth-satellite OGO 3 it is appropriate that attention is directed toward several salient features of the instrumentation and of the orbit. OGO 3 (1966-49A) was launched on 7 June 1966 into a highly eccentric orbit with initial apogee 128,500 km and perigee 6,700 km geocentric radial distances, inclination 31° and period 48.6 hours. At launch the geocentric local time of the direction of the line of apsides was ~ 22:00. A composite system of reaction wheels and gas jets provided a predetermined, monitored orientation of the various spacecraft coordinates with respect to the directions from the satellite to earth and the sun and with respect to the orbital plane. This attitude system operated normally from launch to 23 July 1966. On 23 July a power inverter associated with the attitude control system failed and the spacecraft was subsequently commanded into a spin-stabilized mode. All data presented here were acquired during the period of normal operation of the attitude system. Coordinates for a typical outbound segment of the trajectory over the range of L-values ~ 3 to 15 during this period are displayed in Figure 4 where λ_m denotes

magnetic latitude, θ_{SM} is solar magnetospheric latitude, and θ_{SE} and φ_{SE} are solar ecliptic latitude and longitude, respectively. Note that the orbit is positioned at low latitudes near local evening over the outbound segments. Reference to Figure 17 provides typical coordinates for inbound segments which are located near local midnight at $\sim$ 10 R_E geocentric radial distances.

The University of Iowa instrumentation includes four cylindrical-plate electrostatic analyzers to select charged particle energy and continuous channel multipliers (Bendix 'channeltrons') as charged particle detectors. A diagram of one of the two pairs of these electrostatic analyzers is shown in Figure 5: P_1, P_2 and P_3 denote three cylindrical curved plates; C_1 and C_2 are the proton and electron analyzers, respectively, since P_2 is biased with a variable, programmed positive voltage; and A and B locate the entrance apertures of two continuous channel multipliers. A more complete description has been given by Frank [1965b, 1967a]. Each of the two pairs of electrostatic analyzers provides simultaneous measurements of the directional intensities of protons and electrons, separately, within the same energy bandpasses over an energy range extending from approximately 100 eV to 50,000 eV. A summary of the proton energy bandpasses for one electrostatic analyzer (LEPEDEA 'A') is provided in Table I. The directions of the fields of view of these two pairs of electrostatic analyzers, designated as LEPEDEA's 'A' and 'B' (LEPEDEA, Low Energy

TABLE I

OGO 3 LEPEDEA PROTON CHANNELS 'A'

ENERGY BANDPASSES*

Proton Channel	Energy Bandpass†
3pA	100 - 160 eV
4pA	220 - 350 eV
5pA	360 - 570 eV
6pA	480 - 760 eV
7pA	740 - 1200 eV
8pA	1.1 - 1.8 keV
9pA	1.8 - 2.9 keV
10pA	3.0 - 4.8 keV
11pA	4.4 - 7.1 keV
12pA	8.1 - 13 keV
13 pA	12 - 19 keV
14 pA	16 - 25 keV
15 pA	31 - 49 keV

*See also Frank [1967c].

†Analyzer constant is 7.8 ev(volt)$^{-1}$

Proton and Electron Differential Energy Analyzer) are orthogonal and are directed parallel to spacecraft body Cartesian axes, +Z (toward earth during normal spacecraft operations) and +Y, respectively. In concluding the foregoing comments concerning the instrumentation we stress that a large fraction of the following observations was possible due to the large geometric factor, and hence low threshold intensity, of the instrument which exceeds those of previously flown electrostatic analyzers directed toward measurements of the solar wind [cf Wolfe, Silva and Myers, 1966] by factors $\gtrsim$ 100.

Distributions of Low-Energy Protons and Electrons in the Earth's Magnetosphere

Several recent measurements of low-energy proton and electron intensities in the earth's outer radiation zone and its immediate environs have revealed heretofore unknown features of the charged particle distributions within the earth's magnetosphere which are intimately associated with such ground-based geophysical phenomena as auroras, geomagnetic storms and very-low-frequency (VLF) electromagnetic radiations. As a large fraction of the observations summarized here were acquired with instrumentation borne on the earth-satellite OGO 3 during the period June through July 1966 the reader is reminded that these measurements were obtained at low magnetic latitudes ($\lambda_m \lesssim 25°$) and in the evening-local midnight quadrant of the magnetosphere. First observations of the distributions of low-energy protons (100 eV $\lesssim$ E $\lesssim$ 50 keV) in the outer zone during a period of relative magnetic quiescence are displayed in Figures 6 and 7 (Frank, 1967b). The directional intensities of protons within the six energy bandpasses $330 \leq E \leq 530$ eV, $450 \leq E \leq 720$ eV, $1.8 \leq E \leq 2.9$ keV, $11 \leq E \leq 18$ keV, $16 \leq E \leq 26$ keV and $30 \leq E \leq 48$ keV have been plotted as functions of magnetic shell parameter L over L-values from 3 to 15. It is easily noted that

(a) the narrow proton maximum at $L \simeq 4$ is predominatly populated by protons with energies $\lesssim 2$ keV, (b) proton ($E \gtrsim 5$ keV) intensities are concentrated in a region extending from $L \simeq 5$ to 10, (c) fine structure exists in the profiles of proton ($E \lesssim 26$ keV) intensities beyond $L \simeq 8$, attributable to temporal and/or spatial variations in intensities, and (d) there is a maximum in proton ($30 \leq E \leq 48$ keV) intensities at $L \simeq 7$, 4.5×10^6 $(cm^2\text{-sec-sr})^{-1}$. The peaks of low-energy proton intensities at $L \simeq 4$ are a transient and variable feature of the distribution of charged particles in this region. Although the large low-energy proton (and electron) populations summarized here will significantly distort the geomagnetic field and hence influence the labelling of a given spacecraft position with the magnetic coordinates B and L, the magnetic coordinates as derived from magnetic surveys at the earth's surface [Jensen and Cain, 1962] have been adopted throughout the present discussion as reference coordinates in lieu of an eventual model of the geomagnetic field based upon simultaneous magnetometer measurements.

Of immediate interest with respect to these low-energy proton distributions is the behavior of this vast reservoir of energy during a geomagnetic storm; i.e., are these low-energy protons the predominant population of the storm-time extraterrestrial ring current and hence responsible for the world-wide decrease of the magnetic field intensity observed at low and middle latitudes at the earth's

surface during magnetic storms. Hourly $D_{ST}(H)$ values for the period covering a moderate magnetic storm during early-July 1966 and perigee crossings (P) when measurements of the low-energy proton populations in the outer radiation zone were possible are shown in Figure 8. Note that observations during the main phase of the event were fortuitously obtained. The distributions of protons ($31 \leq E \leq 49$ keV) at low magnetic latitudes and for $1 \lesssim L \lesssim 8$ during the early-July magnetic storm are summarized in Figure 9 which displays directional intensities of protons within the above energy range as functions of magnetic shell parameter L for a series of four homogeneous (i.e., for a given L-value the satellite position and directions of fields of view differ by $\lesssim 5°$) inbound passes during pre-storm, main phase, recovery phase and post-storm conditions. All four profiles of directional intensities share the same ordinate scales to facilitate comparison of the spatial distributions of these protons during various eras of this geomagnetic storm. It is evident upon perusal of Figure 9 that (1) the measurable pre-storm distribution of proton ($31 \leq E \leq 49$ keV) intensities is confined to $L \gtrsim 4.5$, (2) a severe increase in proton ($31 \leq E \leq 49$ keV) directional intensities over $2.9 \lesssim L \lesssim 5.5$ is apparent in the main phase observations on 9 July 1966 with a maximum in intensities located at $L \simeq 3.6$, (3) by 11 July (recovery phase) this proton distribution has substantially decreased in intensities with a peak intensity now positioned at $L \simeq 4.5$ and

(4) during the post-storm period of 13 July the proton distribution is grossly characterized by pre-storm, or quiescent period, intensities. In order to establish that these proton (200 eV $\leq$ E $\leq$ 50 keV) intensities within the earth's outer radiation zone are not only positively correlated with increasing magnitude of $D_{ST}(H)$ but are in fact the predominant contributors to the extraterrestrial ring current providing the depression of the geomagnetic field at low and middle latitudes on the earth's surface during magnetic storms it is necessary to demonstrate that the total energy of this host of charged particles is adequate to account for the disturbance field. It has been previously shown that the total energy of charged particles within the earth's magnetosphere is proportional to the magnitude of the decrease of the horizontal intensity of the magnetic field on the earth's surface at the equator [Dessler and Parker, 1959; Parker, 1966; Sckopke, 1966]. In order to evaluate the total energy of the low-energy proton (and electron) distributions it is necessary to expand the 'snapshots' of Figure 9 into meridional cross-sections of the energy density contours in a R-λ_m coordinate system by approximating the latitude dependence of the energy densities via utilization of simultaneous observations of the directional intensities at two pitch angles at a given L-value (see Frank [1967c] for a detailed discussion of these calculations). An example of the meridional cross-sections of proton energy density contours for the main phase of the early-

July magnetic storm is shown in Figure 10. The total energy of the proton (200 eV $\leq$ E $\leq$ 50 keV) distribution is then obtained by numerical integration of the contours displayed in Figure 10 with the assumption of an azimuthally symmetric ring current. A tabular comparison of the calculated and the observed decreases, $\Delta B(o)$ and $D_{ST}(H)$, respectively, of the magnetic field intensity at the earth's surface near the equator, neglecting the diamagnetism of the earth, for the main phases of two moderate magnetic storms and a typical quiescent period is provided in Table II. The calculated charged-particle total energies, and hence the calculated $\Delta B(o)$, are judged to be accurate to within $\pm$ 50% (refer to Frank [1967c]). Inspection of the calculated and observed magnitudes of the decreases of field intensities at the earth's surface shown in Table II firmly establishes that (1) protons (200 eV $\lesssim$ E $\lesssim$ 50 keV) are the principal contributors to the storm-time extraterrestrial ring current and (2) electrons (200 eV $\lesssim$ E $\lesssim$ 50 keV) are substantial, though lesser contributors, $\sim$ 20% of the total ring current, a result which is in qualitative agreement with earlier measurements with CdS crystals borne on Explorer 12 [Frank, 1966b].

The observations reported above are insufficient to delineate the mechanism, or combination of mechanisms, which is responsible for the transport of charged particles of the extraterrestrial ring current from the distant magnetosphere to locations deep within the

TABLE II

REPRESENTATIVE TOTAL PROTON (200 eV $\leq$ E $\leq$ 50 keV) AND ELECTRON (200 eV $\leq$ E $\leq$ 50 keV) ENERGIES WITHIN THE EARTH'S RADIATION ZONES*

Date	Charged Particles	Charged Particle Total Energy $1 \leq L \leq 8$ (ergs)	$\Delta B(o)$ Calculated (gammas)	$D_{ST}(H)$ Observed (gammas)
23 June 1966	Protons (200 eV $\leq$ E $\leq$ 50 keV)	4.8×10^{21}	-12	Quiescent
25 June 1966	Protons (200 eV $\leq$ E $\leq$ 50 keV)	1.4×10^{22}	-36	-30($\pm$10)
9 July 1966	Protons (200 eV $\leq$ E $\leq$ 50 keV)	2.1×10^{22}	-55	-50($\pm$10)
	Electrons (200 eV $\leq$ E $\leq$ 50 keV)	5.3×10^{21}	-14	

*See also Frank [1967c].

earth's magnetosphere or, alternatively, for the acceleration of lower energy protons ($E \lesssim 100$ eV) to energies $\sim$ tens of keV on a given L-shell. The interpretation of these results in terms of a specific acceleration mechanism is precluded by the necessity of simultaneous measurements of electric fields and magnetic field fluctuations and of the lower energy (ambient) plasma in these regions. However, several observations of proton and electron densities within the outer radiation zone which are already available in the literature appear worthy of discussion in relationship to the extraterrestrial ring current. Carpenter [1963; 1966] has inferred from ground-based studies of whistler propagation through the outer radiation zone that a 'knee' in the electron densities near the magnetic equatorial plane is a persistent feature of the outer radiation zone and has denoted the region of higher electron densities, $\sim 100\ (cm)^{-3}$, (see Figure 11) as the plasmasphere. Of direct interest in the present discussion is the position of the outer surface of the plasmasphere, or plasmapause. Comparison of the position of the plasmapause depicted in Figure 11 with that of the earthward boundary of the extraterrestrial ring current during a moderate storm as shown in Figure 10 suggests that these two 'boundaries' may coincide. Several other observations tend to support this suggestion. Recent observations of the thermal ion densities with a satellite-borne positive-ion spectrometer [Taylor, Brinton and Smith, 1965] support the existence of a plateau in ion

densities (the plasmasphere) and the inverse correlation of the position of the 'knee' with magnetic activity (see Figure 12) previously reported by Carpenter [1966]. The spectrometer results show that this ion belt contracts and expands over an L-value range extending from $L \simeq 3.0$ during periods of high geomagnetic activity to $L \simeq 5 - 6$ during intervals of relative magnetic quiescence [Taylor, et al, 1965]. The positions of the inner edge of the extraterrestrial ring current during the main phases of two moderate magnetic storms and a period of relative magnetic quiescence are summarized in Figure 13 which displays proton ($200\ eV \leq E \leq 50\ keV$) energy densities at the magnetic equator as functions of shell parameter L for these three periods. Of particular note are the positions of peak energy densities at $L \simeq 6.5$ on 23 June 1966 (relative magnetic quiescence), at $L \simeq 4.5$ on 25 June ($D_{ST}(H) \simeq -30\gamma$) and at $L \simeq 3.2$ on 9 July ($D_{ST}(H) - 50\gamma$) and the corresponding <u>decreasing</u> radial distance of the position of the extraterrestrial ring current with <u>increasing</u> geomagnetic activity [Frank, 1967c]. These measurements of the extraterrestrial ring current and of the positive ion belt strongly suggest that the plasmapause and the earthward boundary of the low-energy charged particle populations which dominate the ring current are intimately related. One observational problem which remains unresolved is posed by the energy density contours of protons ($200\ eV \leq E \leq 50\ keV$) and electrons ($200\ eV \leq E \leq 50\ keV$) as functions of L during the main phase of the moderate

geomagnetic storm of early-July shown in Figure 14. One salient result of these measurements establishes that the peak proton (200 eV $\leq$ E $\leq$ 50 keV) energy densities before the rapid decrease with decreasing L on the earthward edge of the ring current at L $\sim$ 3.2 lies deeper within the magnetosphere than the corresponding position for the electron (200 eV $\leq$ E $\leq$ 50 keV) energy densities at L $\sim$ 4.0. Does the position of the plasmapause correspond to the earthward boundary of the electron or proton distributions, or perhaps the positions of the plasmapause inferred from whistler (electron) observations and spectrometer (positive ion) measurements differ at least during geomagnetic storms? Future simultaneous measurements of the ion belt and of the charged particles of the extraterrestrial ring current are mandatory in order to establish the relationship suggested above and, if any, to interpret the signature of the proton and electron energy density contours in terms of local acceleration of thermal plasma or of large-scale plasma convection within the magnetosphere.

An initial investigation of the temporal variations of outer zone electron spectrums over the energy range ~ 100 eV to 50 keV during geomagnetic storms has extended knowledge of these electron spectrums to electron energies heretofore unobserved within the heart of the outer zone. The high energy 'tail' (E $\gtrsim$ 50 keV) of this electron distribution has been studied in detail over the past several years (cf Figure 3); first observations of the low-energy electron spectrums in the outer radiation zone are summarized in Figure 15. The directional, integral intensities of electrons, J(> E), above

300 eV on 23 June 1966 (relative magnetic quiescence) and 25 June (main phase of a moderate magnetic storm) at several L-values shown in Figure 15 are typical of the storm-time variations of low-energy electron spectrums. For reference to the corresponding distribution of low-energy protons during this period the reader is referred to the previous Figure 13. Principal features of these observations are (1) an enhancement of integral intensities by factors $\lesssim 40$ over $L \simeq 4$ to 6 during the magnetic storm, (2) a concurrent softening of the electron integral spectrums for electrons with energies $\gtrsim$ several keV, and (3) enhancements of differential intensities of electrons which are greatest for electron energies ~ several keV to several tens of keV. The electron energy spectrum deeper within the outer radiation zone at $L = 3.4$ remained substantially unaffected by the storm-time activity. These introductory comments concerning storm-time variations of the outer zone electron spectrums will be followed in the future with an intensive investigation of observations and a discussion of their significance in delineating the nature of the acceleration mechanism.

Several researches conducted over the past several years have been directed toward studies of the sharp decrease in electron ($E \sim 50$ keV) intensities with increasing L-value at $L \sim 8$ in the dark hemisphere of the magnetosphere at low and moderate latitudes [cf O'Brien, 1963; Frank, Van Allen and Craven, 1964; McDiarmid and Burrows, 1964; Frank, 1965a; Fritz and Gurnett, 1965]. An example of this precipitous

decrease in electron intensities at $L \sim 5.7$ and low altitudes, $\sim$ 1,000 km, is shown in Figure 16 [Fritz and Gurnett, 1965] which also displays the relationship of this boundary to an intense flux of lower energy electrons ($E \geq 10$ keV) at higher latitudes. This position of the sharp decrease in electron ($E \sim 50$ keV) intensities with increasing L has often been termed the 'trapping boundary' [cf Frank, 1965a; Craven, 1966]; whether or not it is in fact the outermost limit of durable trapping (i.e., the electrons remain trapped for an entire longitudinal drift period) within the earth's magnetosphere as suggested by the above designation is a problem which remains unresolved. Our initial efforts toward developing a description of the morphology of the low-energy electron (100 eV $\lesssim E \lesssim 50$ keV) distributions within the outer magnetosphere as measured with the OGO 3 electrostatic analyzer array have established several salient features of the intensity distributions near the 'trapping boundary' at local midnight near the magnetic equatorial plane. A typical set of profiles of low-energy electron intensities as functions of shell-parameter L is displayed in Figure 17 during an inbound pass through the outer magnetosphere at low magnetic latitudes near the midnight meridional plane ($\varphi_{SM} = 180°$). These profiles of the directional intensities of electrons ($630 \leq E \leq 1100$ eV, $1.5 \leq E \leq 2.7$ keV, $6.8 \leq E \leq 12$ keV, $27 \leq E \leq 47$ keV and $E > 45$ keV) are remarkably dissimilar with the exception of the region below $L \sim 5$ in the outer

radiation zone and are typical of the observed distributions of intensities in this region. Inspection of Figure 17 reveals the distributions of lower energy electron intensities are positioned with respect to the 'trapping boundary' via a complex and energy-dependent relationship for $L \gtrsim 5$: (1) only a small variation of electron ($27 \leq E \leq 47$ keV) intensities occurs at the 'trapping boundary' at $L \sim 7.0$ coincident with the onset of a large decrease in electron ($6.8 \leq E \leq 12$ keV) intensities with decreasing L, (2) a rapid decrease of intensities of electrons ($1.5 \leq E \leq 2.7$ keV) with decreasing L-value at $L = 6.0$ inside the 'trapping boundary' and (3) a small maximum of electron ($630 \leq E \leq 1100$ eV) intensities inside the 'trapping boundary'. We shall direct our attention herein primarily to the positions of the onset of the near-earth decreases of electron intensities and designate these positions as $L_D(E)$. A series of observations over a similar traversal of this region is displayed in Figure 18. For a given L-value the coordinates α_o (equatorial pitch angle), φ_{SM} (solar magnetospheric longitude) and λ_m (geomagnetic latitude) during this period do not largely differ from those plotted in Figure 17 since the orbital period of the spacecraft is 48.6 hours (2.03 days). A striking feature of the observations during these four passes is the persistent deeper penetration of maximum electron ($1.5 \leq E \leq 2.7$ keV) intensities when compared to the corresponding near-earth onset of decreasing intensities of electrons ($3.8 \leq E \leq 6.8$ keV), or in our

notation L_D ($1.5 \leq E \leq 2.7$ keV) < L_D ($3.8 \leq E \leq 6.8$ keV) (see Frank [1967d] for more examples). A definite position of the onset of a sharp decrease in electron ($14 \leq E \leq 24$ keV) intensities is not usually cognizable but is often positioned at L_D ($14 \leq E \leq 24$ keV) > L_D ($3.8 \leq E \leq 6.8$ keV) when a decrease is apparent (cf Figure 18). The persistent occurrence of greater values of $L_D(E)$ with increasing electron energy within the energy range ~ 1 to 10 keV is demonstrated by the summary offered in Table III which includes K_p for the period of observation of L_D and the corresponding daily sum K_p, ΣK_p [Lincoln, 1966]. The values of L_D vary by several earth radii within the series of observations reported here and display no obvious correlation with K_p or ΣK_p, but the difference $L(3.8 \leq E \leq 6.8$ keV) - $L(1.5 \leq E \leq 2.7$ keV) is usually ~ 0.5 R_E. During the main phase of the moderate geomagnetic storm on 9 July L_D ($1.5 \leq E \leq 2.7$ keV) was located deep within the outer zone at $L \simeq 4.0$ (cf Figure 14). It is of further interest to note that the maximum intensities of electrons ($1 \lesssim E \lesssim 10$ keV) can be located inside the 'trapping boundary', outside the 'trapping boundary', or may straddle this position of the termination of relatively high electron ($E > 45$ keV) intensities near local midnight in the vicinity of the magnetic equatorial plane [Frank, 1967d]. It is noted here that these observations of generally lower energy electrons (see Figures 17 and 18) and higher energy protons (see Figures 6 and 7) with decreasing radial distance over $5 \lesssim L \lesssim 10$ in

TABLE III

OBSERVED VALUES OF THE PARAMETER $L_D(E)$
NEAR THE MIDNIGHT MERIDIONAL PLANE*

Date (inbound pass)	$L_D(1.5 \leq E \leq 2.7$ keV), earth radii	$L_D(3.8 \leq E \leq 6.8$ keV), earth radii	K_p during observation of L_D	Daily Sum K_p (ΣK_p)
27 June 1966	6.2	6.7	0^+	7^-
29 June 1966	7.2	7.5	1^-	11^+
1 July 1966	5.3	5.9	1^+	12^-
3 July 1966	8.4	8.7	1^-	9^+

*See also Frank [1967d].

the evening-midnight quadrant of the magnetosphere are in qualitative agreement with calculations of the adiabatic motion of solar wind protons and electrons in a current model of the geoelectric and geomagnetic fields [Hones, 1963; Taylor and Hones, 1965; Taylor, 1966]. A diagram of the electric equipotentials projected into the equatorial plane is reproduced in the present Figure 19 [Taylor and Hones, 1965]; the region of the observations of low-energy protons and electrons discussed above lies in the (-X, Y) quadrant over geocentric radial distances $\sim$ 5 to 15 R_E. Although the above qualitative agreement is not definitive in terms of delineating this magnetospheric model as an effective approximation of the earth's magnetosphere, it strongly suggests that a geoelectric potential system exercises an important role in the acceleration (deceleration) of charged particles with energies $\lesssim$ several tens of keV within the earth's magnetosphere.

Acknowledgements

This research was supported in part by the National Aeronautics and Space Administration under Grant NsG-233-62 and Contract NAS5-2054 and by the Office of Naval Research under Contract Nonr-1509(06).

References

Carpenter, D. L., Whistler evidence of a 'knee' in the magnetospheric ionization density profile, J. Geophys. Res., 68, 1675-1682, 1963.

Carpenter, D. L., Whistler studies of the plasmapause in the magnetosphere, 1. Temporal variations in the position of the knee and some evidence on plasma motions near the knee, J. Geophys. Res., 71, 693-709, 1966.

Craven, John D., Temporal variations of electron intensities at low altitudes in the outer radiation zone as observed with Satellite Injun 3, J. Geophys. Res., 71, 5643-5663, 1966.

Dessler, A. J. and E. N. Parker, Hydromagnetic theory of geomagnetic storms, J. Geophys. Res., 64, 2239-2252, 1959.

Frank, L. A., A survey of electrons E > 40 keV beyond 5 earth radii with Explorer XIV, J. Geophys. Res., 70, 1593-1626, 1965a.

Frank, L. A., Low-energy proton and electron experiment for the Orbiting Geophysical Observatories B and E, U. of Iowa Res. Rep. 65-22, 1965b.

Frank, L. A., Observations of magnetospheric boundary phenomena, Radiation Trapped in the Earth's Magnetic Field, ed. by B. M. McCormac, D. Reidel Publishing Co., Dordrecht-Holland, pp. 422-446, 1966a.

Frank, L. A., Explorer 12 observations of the temporal variations of low-energy electron intensities in the outer radiation zone during geomagnetic storms, J. Geophys. Res., 71, 4631-4639, 1966b.

Frank, L. A., Initial observations of low-energy electrons in the earth's magnetosphere with OGO 3, J. Geophys. Res., 72, 185-195, 1967a.

Frank, L. A., Several observations of low-energy protons and electrons in the earth's magnetosphere with OGO 3, J. Geophys. Res., 72, 1905-1916, 1967b.

Frank, L. A., On the extraterrestrial ring current during geomagnetic storms, J. Geophys. Res., 72, 3753-3767, 1967c.

Frank, L. A., Recent observations of low-energy charged particles in the earth's magnetosphere, to be published in Proceedings, Summer Institute on Physics of the Magnetosphere, Boston College, 1967d.

Frank, L. A., J. A. Van Allen and J. D. Craven, Large diurnal variations of geomagnetically trapped and of precipitated electrons observed at low altitudes, J. Geophys. Res., 69, 3155-3167, 1964.

Fritz, T. A. and D. A. Gurnett, Diurnal and latitudinal effects observed for 10 keV electrons at low satellite altitudes, J. Geophys. Res., 70, 2485-2502, 1965.

Hones, E. W., Jr., Motions of charged particles trapped in the earth's magnetosphere, J. Geophys. Res., 68, 1209-1219, 1963.

Jensen, D. C. and J. D. Cain, An interim geomagnetic field (abstract), J. Geophys. Res., 67, 3568-3569, 1962.

Lincoln, J. Virginia, Geomagnetic and solar data, J. Geophys. Res., 71, 5211, 5784, 1966.

McCormac, B. M., ed., Radiation Trapped in the Earth's Magnetic Field, D. Reidel Publishing Co., Dordrecht-Holland, 1966.

McDiarmid, I. B. and J. R. Burrows, High-latitude boundary of the outer radiation zone at 1000 km, Can. J. Phys., 42, 616-626, 1964a.

Ness, N. F., C. S. Scearce and J. B. Seek, Initial results of the IMP-1 magnetic field experiment, J. Geophys. Res., 69, 3531-3569, 1964.

O'Brien, B. J., A large diurnal variation of the geomagnetically trapped radiation, J. Geophys. Res., 68, 989-995, 1963.

Owens, H. D. and L. A. Frank, Electron omnidirectional contours in the earth's outer radiation zone, J. Geophys. Res., (accepted for publication), 1967.

Parker, E. N., Particle effects in the geomagnetic field, Radiation Trapped in the Earth's Magnetic field, ed. by B. M. McCormac, D. Reidel Publishing Co., Dordrecht-Holland, 302-320, 1966.

Sckopke, N., A general relation between the energy of trapped particles and the disturbance field near the earth, J. Geophys. Res., 71, 3125-3130, 1966.

Taylor, H. A., Jr., H. C. Brinton and C. R. Smith, Positive ion composition in the magnetoionosphere obtained from the OGO-A satellite, J. Geophys. Res., 70, 5769-5181, 1965.

Taylor, Harold E., Adiabatic motion of outer-zone particles in a model of the geoelectric and geomagnetic fields, J. Geophys. Res., 71, 5135-5147, 1966.

Taylor, H. E. and E. W. Hones, Jr., Adiabatic motion of auroral particles in a model of the electric and magnetic field surrounding the earth, J. Geophys. Res., 70, 3605-3628, 1965.

Wolfe, J. H., R. W. Silva and M. A. Myers, Observations of the solar wind during the flight of IMP 1, J. Geophys. Res., 71, 1319-1340, 1966.

Figure Captions

Figure 1. Coarse summary of low-energy charged particle observations. Average positions of the magnetopause and the shock as given by Ness et al [1964] have been included in this diagram (after Frank [1966a]).

Figure 2. Coarse summary of the observations of electrons $E > 40$ keV near the ecliptic plane (after Frank [1966a]).

Figure 3. Contours of constant omnidirectional intensities of electrons ($E > 40$ keV, > 230 keV, and > 1.6 MeV) at the magnetic equator during October through November 1962 (after [Owens and Frank, 1967]). Daily sum K_p has been included at bottom of this figure to indicate levels of geomagnetic activity.

Figure 4. Several useful position coordinates for OGO 3 on 15 June 1966 (outbound pass) (after Frank [1967b]).

Figure 5. Diagram of the basic mechanical features of the OGO 3 Low Energy Proton and Electron Differential Energy Analyzer (abbreviation, LEPEDEA) (after Frank [1967a]).

Figure 6. Unidirectional intensities of protons ($330 \leq E \leq 530$ eV, $450 \leq E \leq 720$ eV and $1.8 \leq E \leq 2.9$ keV) as functions of L for the outbound OGO 3 traversal of the outer radiation zone on 15 June 1966. Intensities are plotted as ●, upper limits as O (after Frank [1967b]).

Figure 7. Continuation of Figure 6 for protons ($11 \leq E \leq 18$ keV, $16 \leq E \leq 26$ keV and $30 \leq E \leq 48$ keV) (after Frank [1967b]).

Figure 8. Hourly $D_{ST}(H)$ values for the period covering the geomagnetic storm during early July 1966 (after Frank [1967c]).

Figure 9. Directional intensities of protons ($31 \leq E \leq 49$ keV) as functions of L at low magnetic latitudes during the pre-storm, main phase, recovery phase and post-storm periods of the early-July geomagnetic storm (after Frank [1967c]).

Figure 10. Contours of constant proton (200 eV $\leq E \leq$ 50 keV) energy densities in a R-λ_m coordinate system on 9 July 1966 (after Frank [1967c]).

Figure 11. Idealized meridian cross section of the magnetosphere near 1400 LT. The shaded region shows the location of the high-density plasma inside the plasmapause. The dashed part of the boundary shows the low altitude region in which the structure of the knee is not well known. The magnetic condition represented is one of moderate but steady agitation (K_p=2-4) (after Carpenter [1966]).

Figure 12. Correlation between three N_i plateaus obtained at varying geomagnetic coordinates and the knee in the equatorial profile of N_e determined from whistler data. The inverse relationship between plateau altitude and A_p is demonstrated (after Taylor, Brinton and Smith [1965]).

Figure 13. Proton (200 eV $\leq$ E $\leq$ 50 keV) energy densities as functions of L at the geomagnetic equator (λ_m = 0°) during two moderate geomagnetic storms on 25 June and 9 July. The energy density profile for 23 June is a typical signature of the quiet-time proton (200 eV $\leq$ E $\leq$ 50 keV) distributions in the evening sector of the earth's magnetosphere (after Frank [1967c]).

Figure 14. Electron (200 eV $\leq$ E $\leq$ 50 keV) and proton (200 eV $\leq$ E $\leq$ 50 keV) energy densities as functions of L during the main phase of the early-July storm (after Frank [1967c]).

Figure 15. Several directional, integral energy spectrums of low-energy electrons at selected L-values during relatively quiescent (●) and moderately disturbed (0) periods. The local pitch angles α for these directional intensities are given for each L-value.

Figure 16. An example of a southbound pass demonstrating the large amount of softening of the electron energy spectrum between 10 and 40 keV associated with the 40 keV trapping boundary (after Fritz and Gurnett [1965]).

Figure 17. Directional intensities of electrons (630 $\leq$ E $\leq$ 1100 eV, 1.5 $\leq$ E $\leq$ 2.7 keV, 6.8 $\leq$ E $\leq$ 12 keV, 27 $\leq$ E $\leq$ 47 keV and E > 45 keV) observed during an inbound pass through the outer magnetosphere near the midnight meridional plane on 22-23 June 1966 (after Frank [1967d]).

Figure 18. Continuation of Figure 17 for directional intensities of electrons ($1.5 \leq E \leq 2.7$ keV, $3.8 \leq E \leq 6.8$ keV, $14 \leq E \leq 24$ keV, and $E > 45$ keV) on 1 July 1966 (after Frank [1967d]).

Figure 19. Electric potentials mapped into the equatorial plane viewed from above the north pole (after Taylor and Hones [1965]).

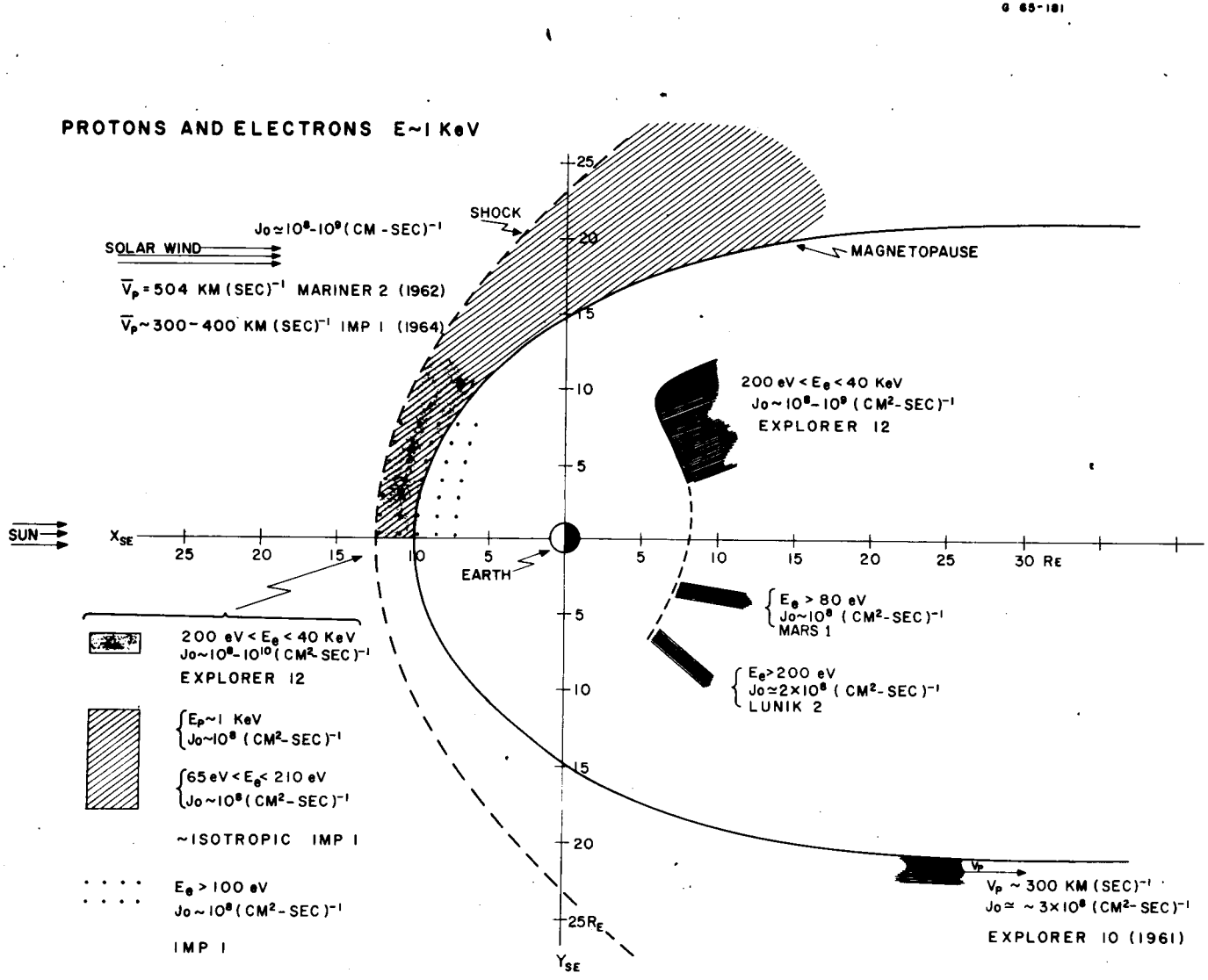
G 65-181
PROTONS AND ELECTRONS E~1 KeV
SHOCK
Jo≃10⁸-10⁹(CM-SEC)⁻¹
SOLAR WIND
$\bar{V}_p$=504 KM(SEC)⁻¹ MARINER 2 (1962)
$\bar{V}_p$~300-400 KM(SEC)⁻¹ IMP 1 (1964)
MAGNETOPAUSE
200 eV < Eₑ < 40 KeV
Jo~10⁸-10⁹ (CM²-SEC)⁻¹
EXPLORER 12
SUN
X_{SE}
25 20 15 10 5 EARTH 5 10 15 20 25 30 RE
25 20 15 10 5 10 15 20 25 R_E
Y_{SE}
Eₑ > 80 eV
Jo~10⁸ (CM²-SEC)⁻¹
MARS 1
Eₑ > 200 eV
Jo≃2×10⁸ (CM²-SEC)⁻¹
LUNIK 2
200 eV < Eₑ < 40 KeV
Jo~10⁸-10¹⁰ (CM²-SEC)⁻¹
EXPLORER 12
Eₚ~1 KeV
Jo~10⁸ (CM²-SEC)⁻¹
65 eV < Eₑ < 210 eV
Jo~10⁸ (CM²-SEC)⁻¹
~ISOTROPIC IMP 1
Eₑ > 100 eV
Jo~10⁸ (CM²-SEC)⁻¹
IMP 1
V_p
V_p ~ 300 KM(SEC)⁻¹
Jo≃ ~3×10⁸ (CM²-SEC)⁻¹
EXPLORER 10 (1961)

Figure 1

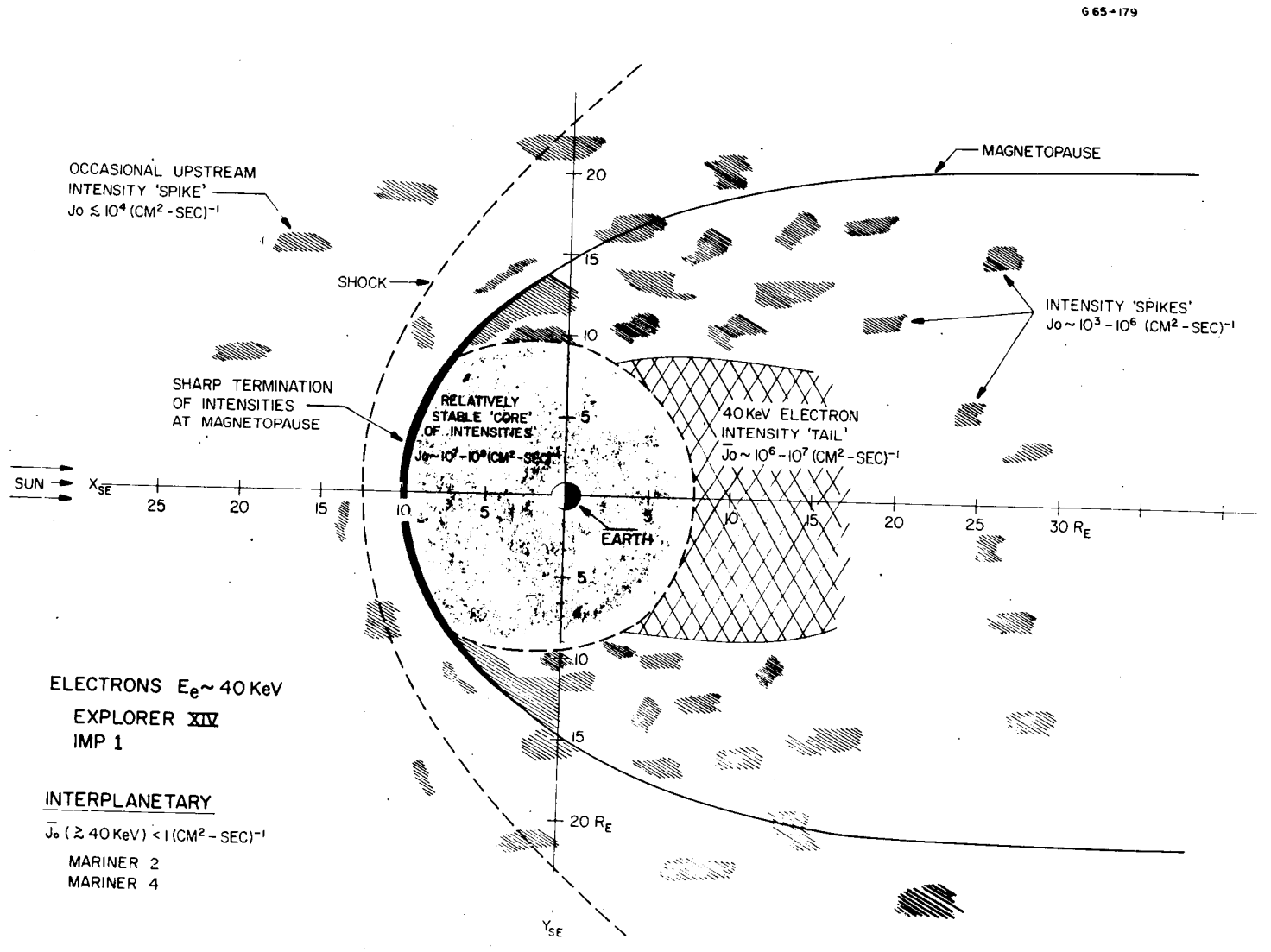
G 65-179
OCCASIONAL UPSTREAM
INTENSITY 'SPIKE'
Jo ≲ 10⁴ (CM² - SEC)⁻¹
SHOCK
MAGNETOPAUSE
INTENSITY 'SPIKES'
Jo ~ 10³ - 10⁶ (CM² - SEC)⁻¹
SHARP TERMINATION
OF INTENSITIES
AT MAGNETOPAUSE
RELATIVELY
STABLE 'CORE'
OF INTENSITIES
Jo ~ 10⁷ - 10⁸ (CM² - SEC)⁻¹
40 KeV ELECTRON
INTENSITY 'TAIL'
J̄o ~ 10⁶ - 10⁷ (CM² - SEC)⁻¹
SUN
X_SE
EARTH
30 R_E
20 R_E
Y_SE
ELECTRONS E_e ~ 40 KeV
EXPLORER XIV
IMP 1
INTERPLANETARY
J̄o (≳ 40 KeV) < 1 (CM² - SEC)⁻¹
MARINER 2
MARINER 4

Figure 2

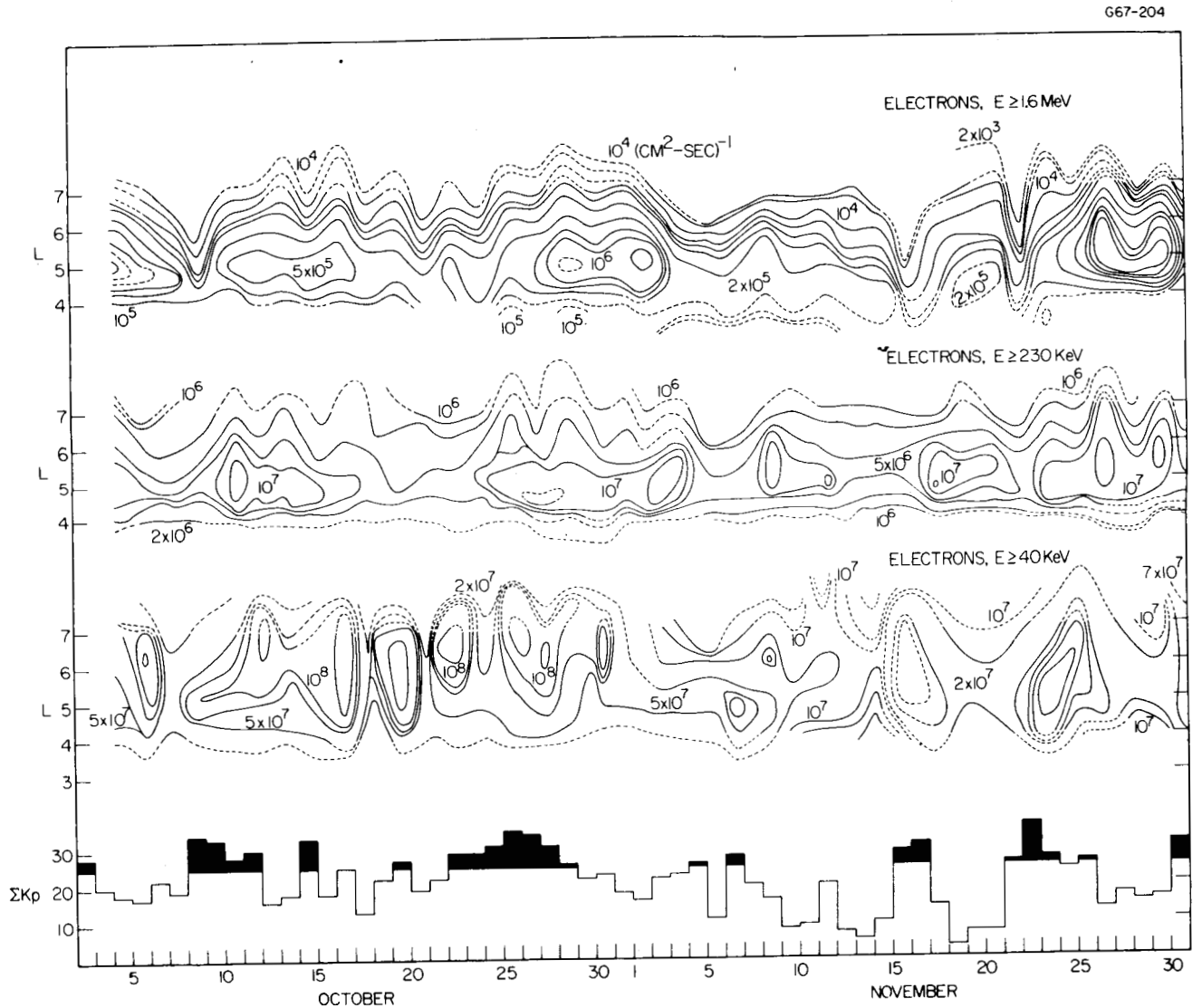
G67-204
ELECTRONS, E ≥ 1.6 MeV
10^4 (CM^2-SEC)$^{-1}$
ELECTRONS, E ≥ 230 KeV
ELECTRONS, E ≥ 40 KeV
L
ΣKp
OCTOBER
NOVEMBER

Figure 3

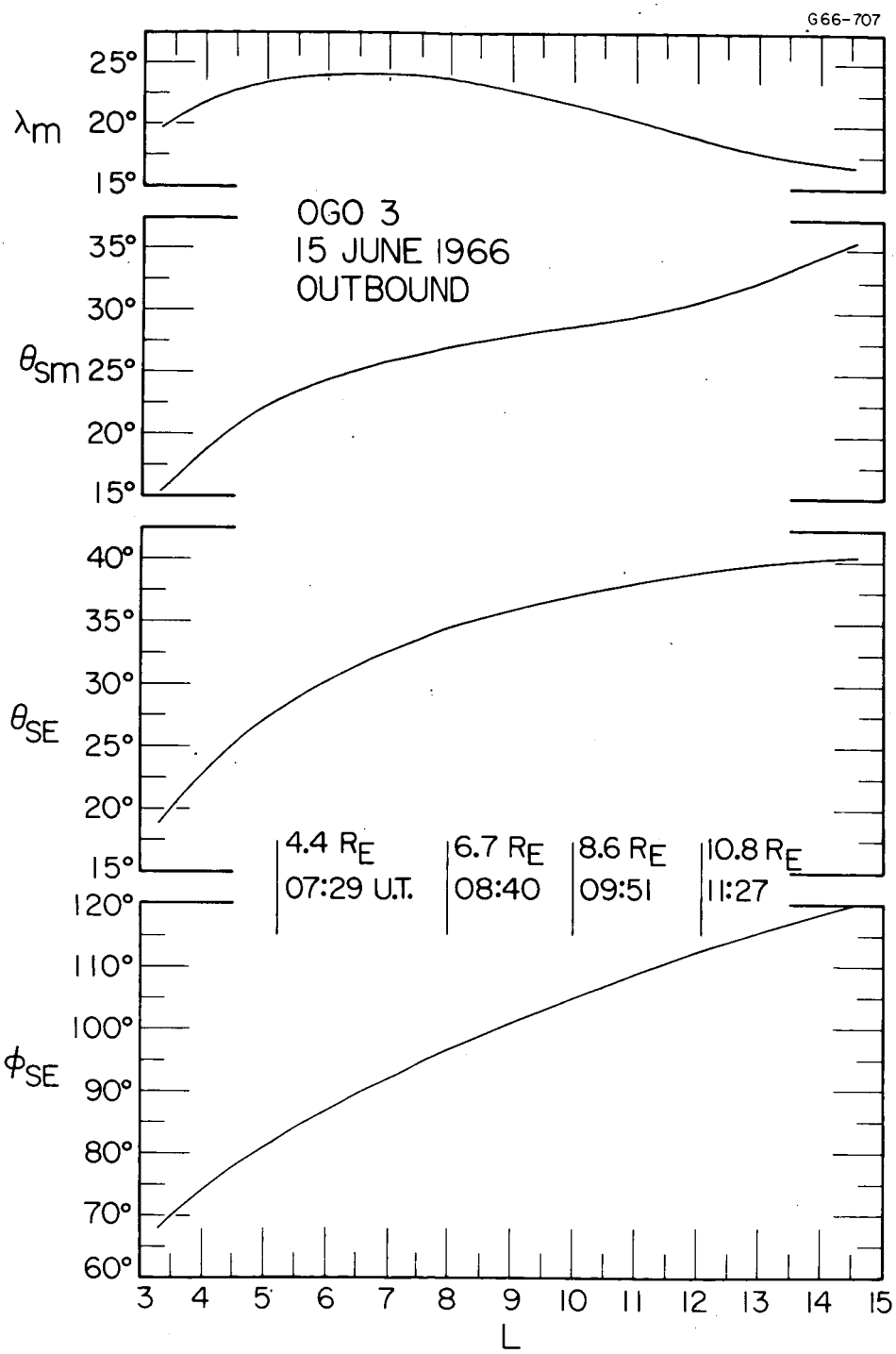
G66-707
λm
25°
20°
15°
OGO 3
15 JUNE 1966
OUTBOUND
θsm
35°
30°
25°
20°
15°
θSE
40°
35°
30°
25°
20°
15°
4.4 RE
07:29 U.T.
6.7 RE
08:40
8.6 RE
09:51
10.8 RE
11:27
φSE
120°
110°
100°
90°
80°
70°
60°
3 4 5 6 7 8 9 10 11 12 13 14 15
L

Figure 4

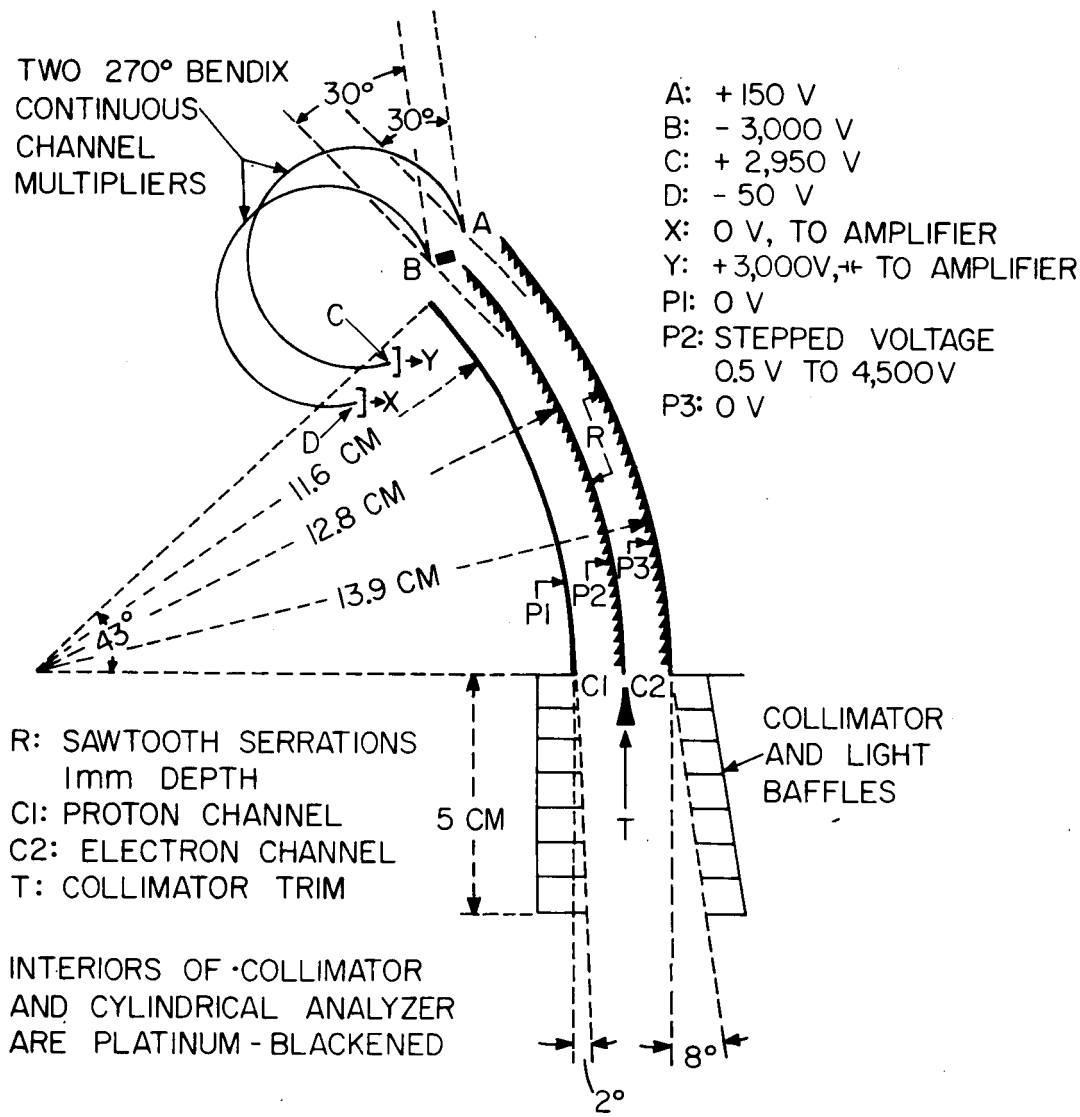
TWO 270° BENDIX CONTINUOUS CHANNEL MULTIPLIERS
30°
30°
A
B
C
Y
X
D
11.6 CM
12.8 CM
13.9 CM
43°
R
P1
P2
P3
C1
C2
5 CM
T
COLLIMATOR AND LIGHT BAFFLES
A: + 150 V
B: - 3,000 V
C: + 2,950 V
D: - 50 V
X: 0 V, TO AMPLIFIER
Y: +3,000V, TO AMPLIFIER
P1: 0 V
P2: STEPPED VOLTAGE 0.5 V TO 4,500V
P3: 0 V
R: SAWTOOTH SERRATIONS 1mm DEPTH
C1: PROTON CHANNEL
C2: ELECTRON CHANNEL
T: COLLIMATOR TRIM
INTERIORS OF COLLIMATOR AND CYLINDRICAL ANALYZER ARE PLATINUM - BLACKENED
8°
2°

Figure 5

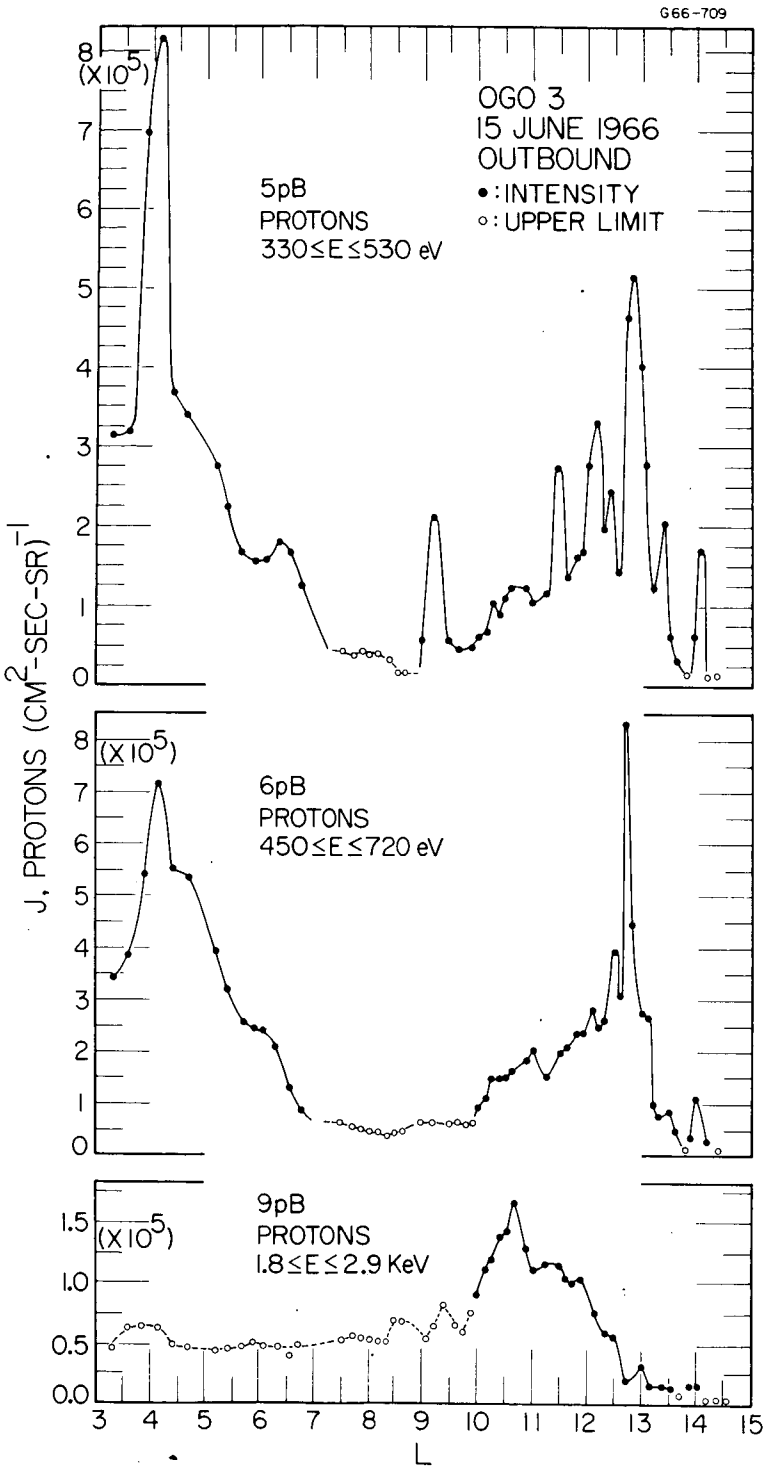
G66-709
OGO 3
15 JUNE 1966
OUTBOUND
•: INTENSITY
○: UPPER LIMIT
5pB
PROTONS
330≤E≤530 eV
6pB
PROTONS
450≤E≤720 eV
9pB
PROTONS
1.8≤E≤2.9 KeV
(X10^5)
J, PROTONS (CM^2-SEC-SR)^-1
L

Figure 6

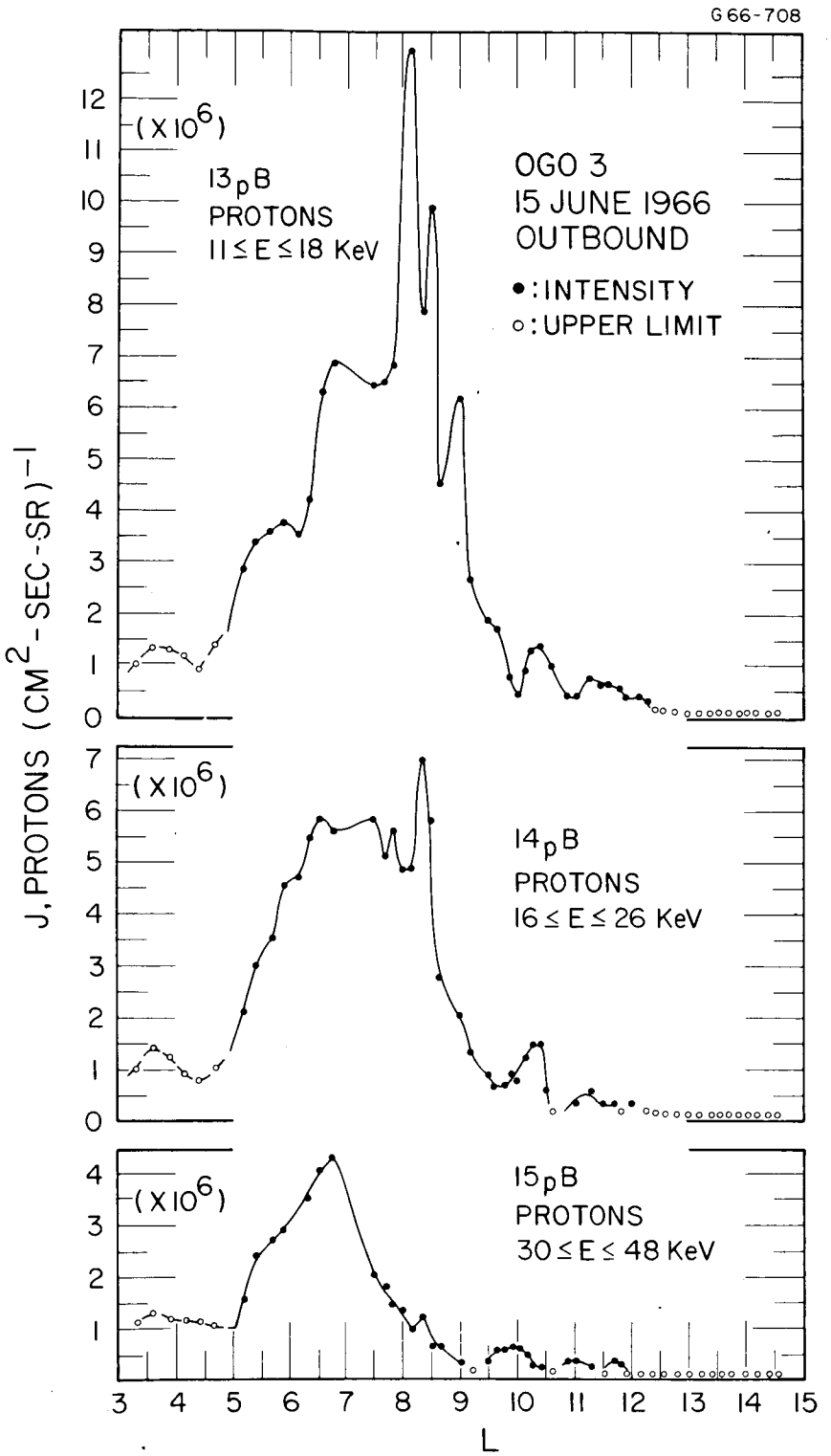
G66-708
J, PROTONS (CM^2-SEC-SR)$^{-1}$
(X10^6)
$^{13}_{p}$B
PROTONS
11 ≤ E ≤ 18 KeV
OGO 3
15 JUNE 1966
OUTBOUND
●: INTENSITY
○: UPPER LIMIT
(X10^6)
$^{14}_{p}$B
PROTONS
16 ≤ E ≤ 26 KeV
(X10^6)
$^{15}_{p}$B
PROTONS
30 ≤ E ≤ 48 KeV
L

Figure 1

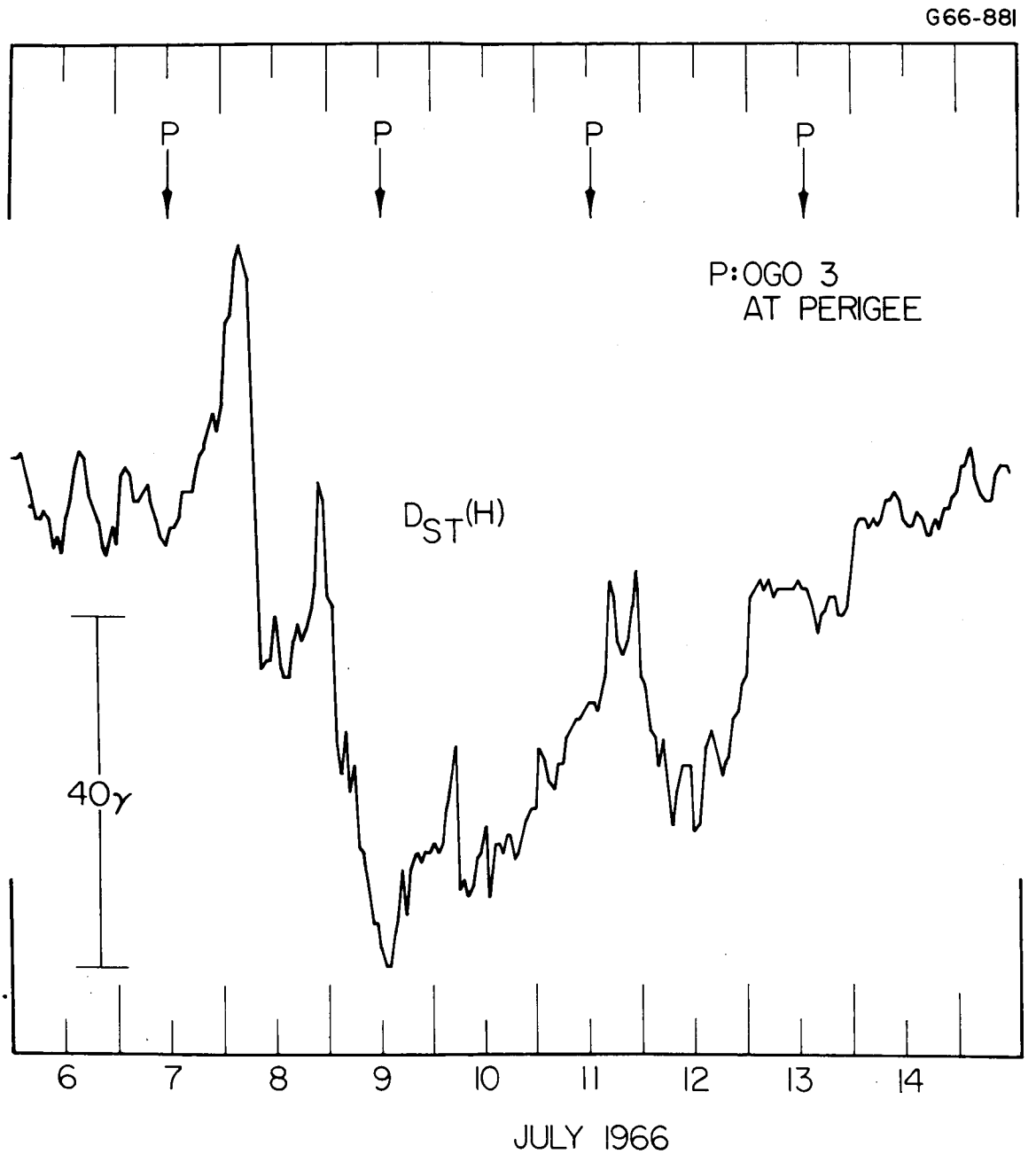
G66-881
P
P
P
P
P:OGO 3
AT PERIGEE
$D_{ST}(H)$
40γ
6
7
8
9
10
11
12
13
14
JULY 1966

Figure 8

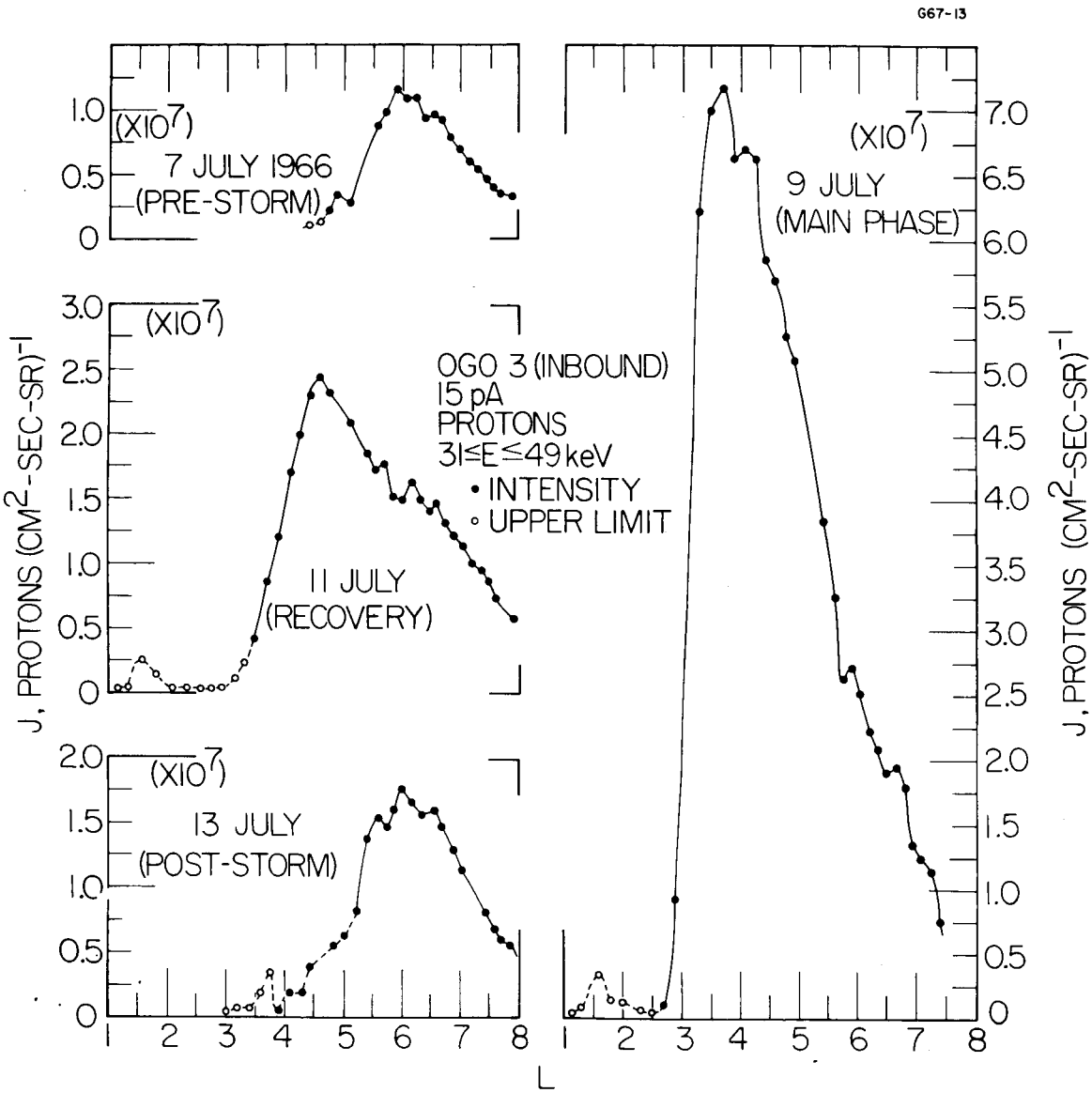
G67-13
(X10^7)
7 JULY 1966
(PRE-STORM)
(X10^7)
11 JULY
(RECOVERY)
OGO 3 (INBOUND)
15 pA
PROTONS
31≤E≤49 keV
• INTENSITY
◦ UPPER LIMIT
(X10^7)
13 JULY
(POST-STORM)
(X10^7)
9 JULY
(MAIN PHASE)
J, PROTONS (CM^2-SEC-SR)^-1
J, PROTONS (CM^2-SEC-SR)^-1
L

Figure 9

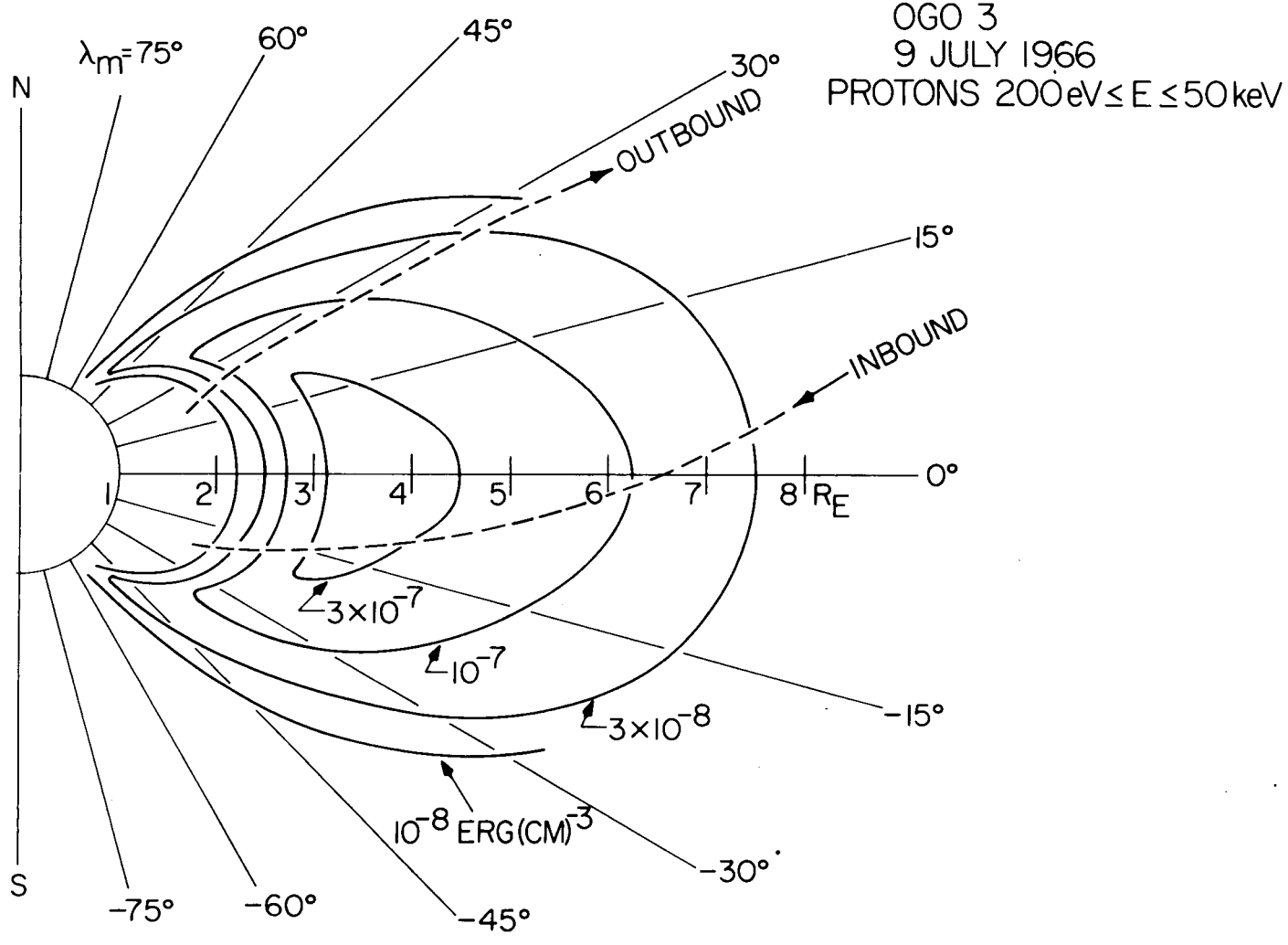
OGO 3
9 JULY 1966
PROTONS 200eV≤E≤50keV
N
S
λ_m=75°
60°
45°
30°
15°
0°
-15°
-30°
-45°
-60°
-75°
OUTBOUND
INBOUND
1
2
3
4
5
6
7
8
R_E
3×10^{-7}
10^{-7}
3×10^{-8}
10^{-8} ERG(CM)$^{-3}$

Figure 10

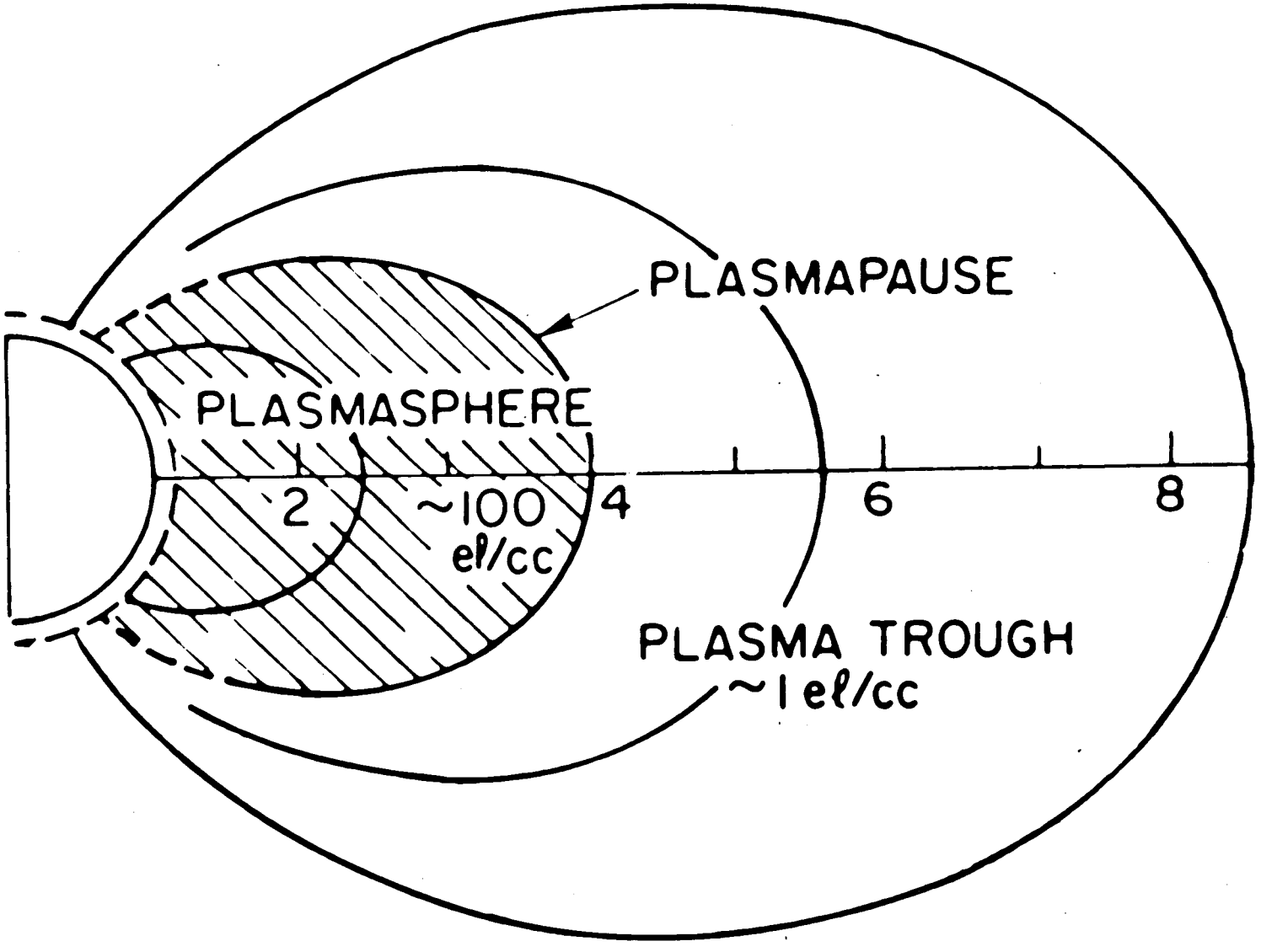
PLASMAPAUSE
PLASMASPHERE
2
~100
el/cc
4
6
8
PLASMA TROUGH
~1 el/cc

Figure 11

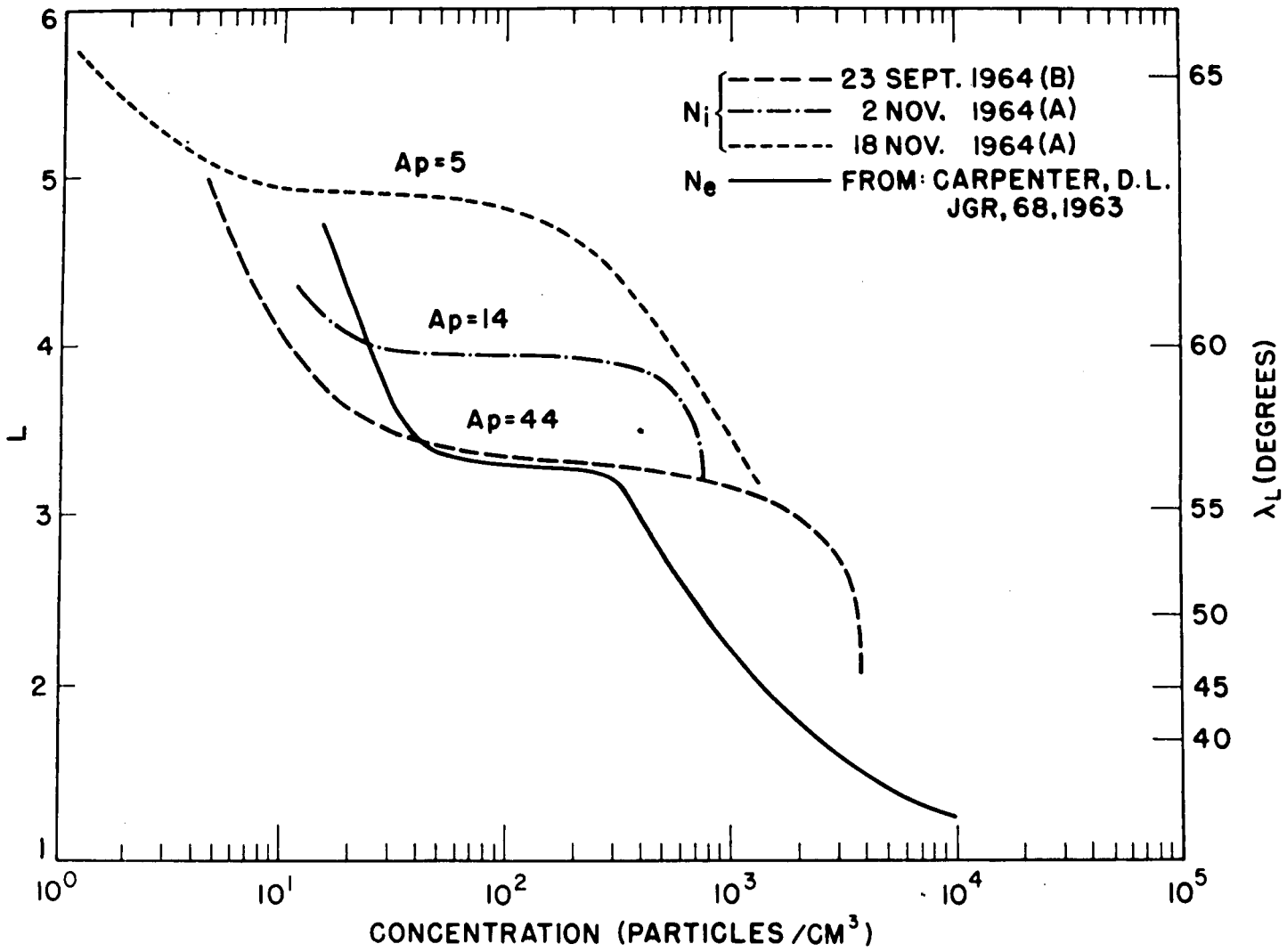
6
5
4
3
2
1
L
65
60
55
50
45
40
λ_L (DEGREES)
10^0
10^1
10^2
10^3
10^4
10^5
CONCENTRATION (PARTICLES/CM^3)
N_i
23 SEPT. 1964 (B)
2 NOV. 1964 (A)
18 NOV. 1964 (A)
N_e
FROM: CARPENTER, D.L. JGR, 68, 1963
Ap=5
Ap=14
Ap=44

Figure 12

G67-27

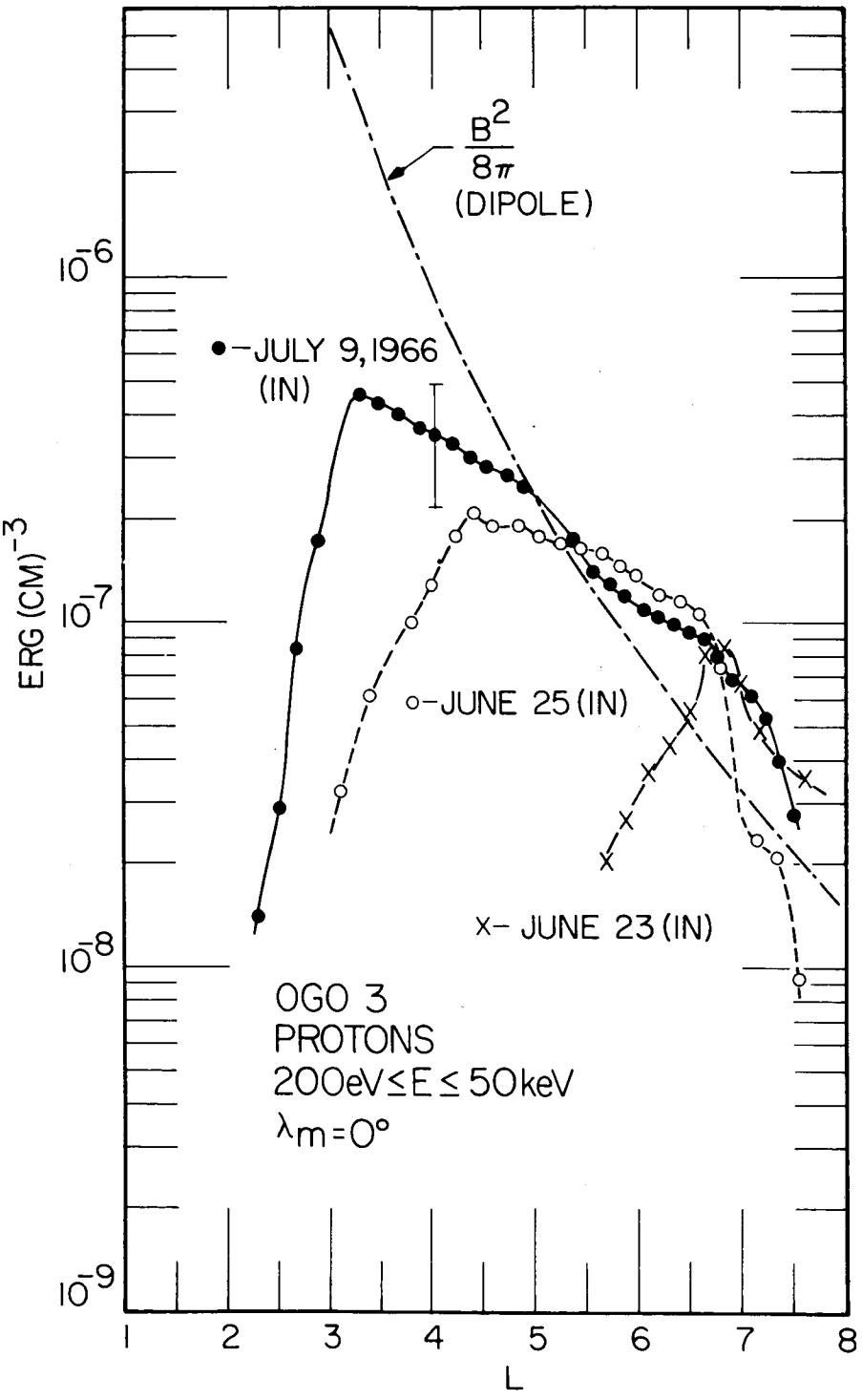

Figure 13

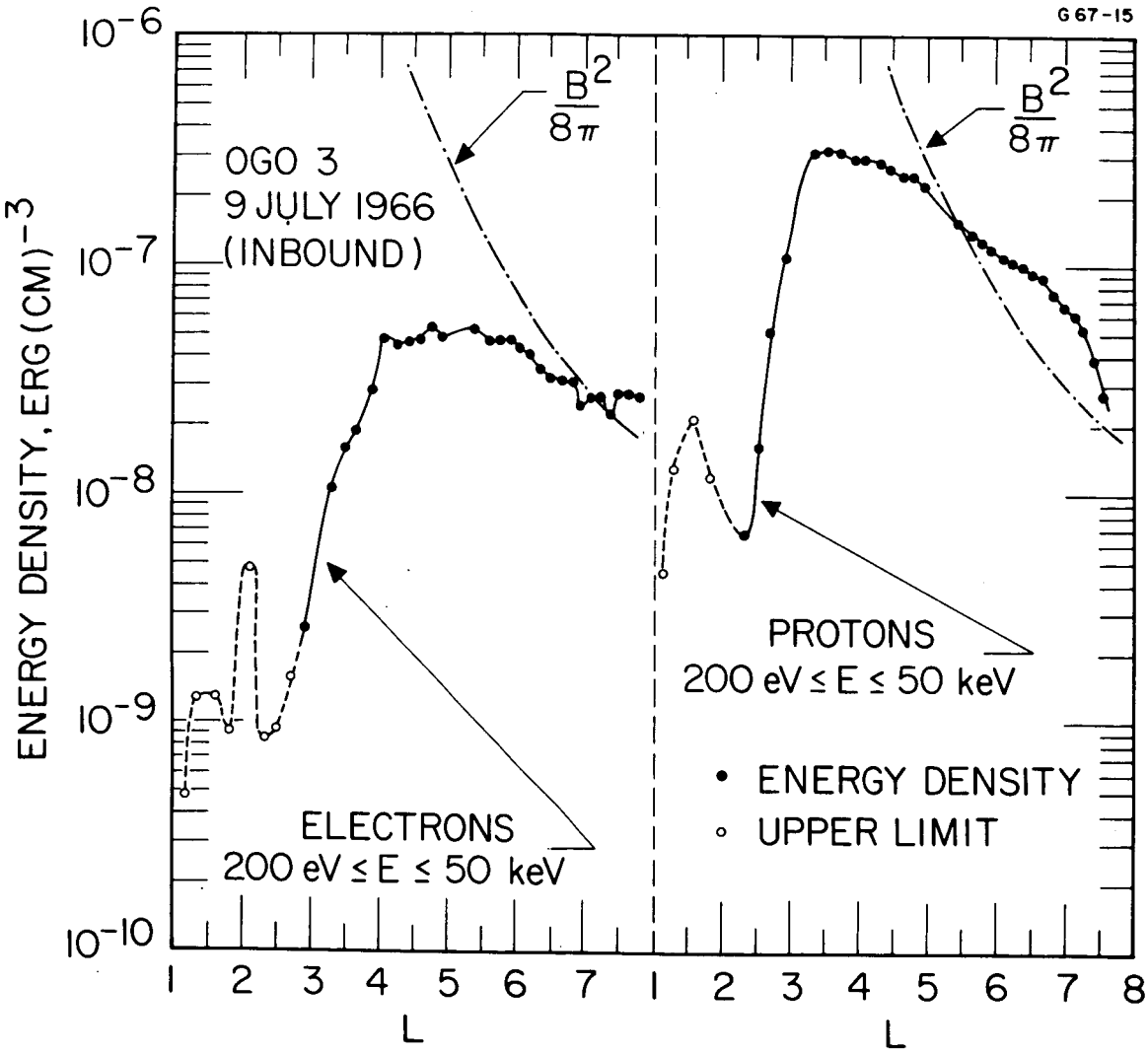
G 67-15
ENERGY DENSITY, ERG (CM)$^{-3}$
10^{-6}
10^{-7}
10^{-8}
10^{-9}
10^{-10}
$\frac{B^2}{8\pi}$
OGO 3
9 JULY 1966
(INBOUND)
ELECTRONS
200 eV ≤ E ≤ 50 keV
PROTONS
200 eV ≤ E ≤ 50 keV
• ENERGY DENSITY
◦ UPPER LIMIT
1 2 3 4 5 6 7
L
1 2 3 4 5 6 7 8
L

Figure 14

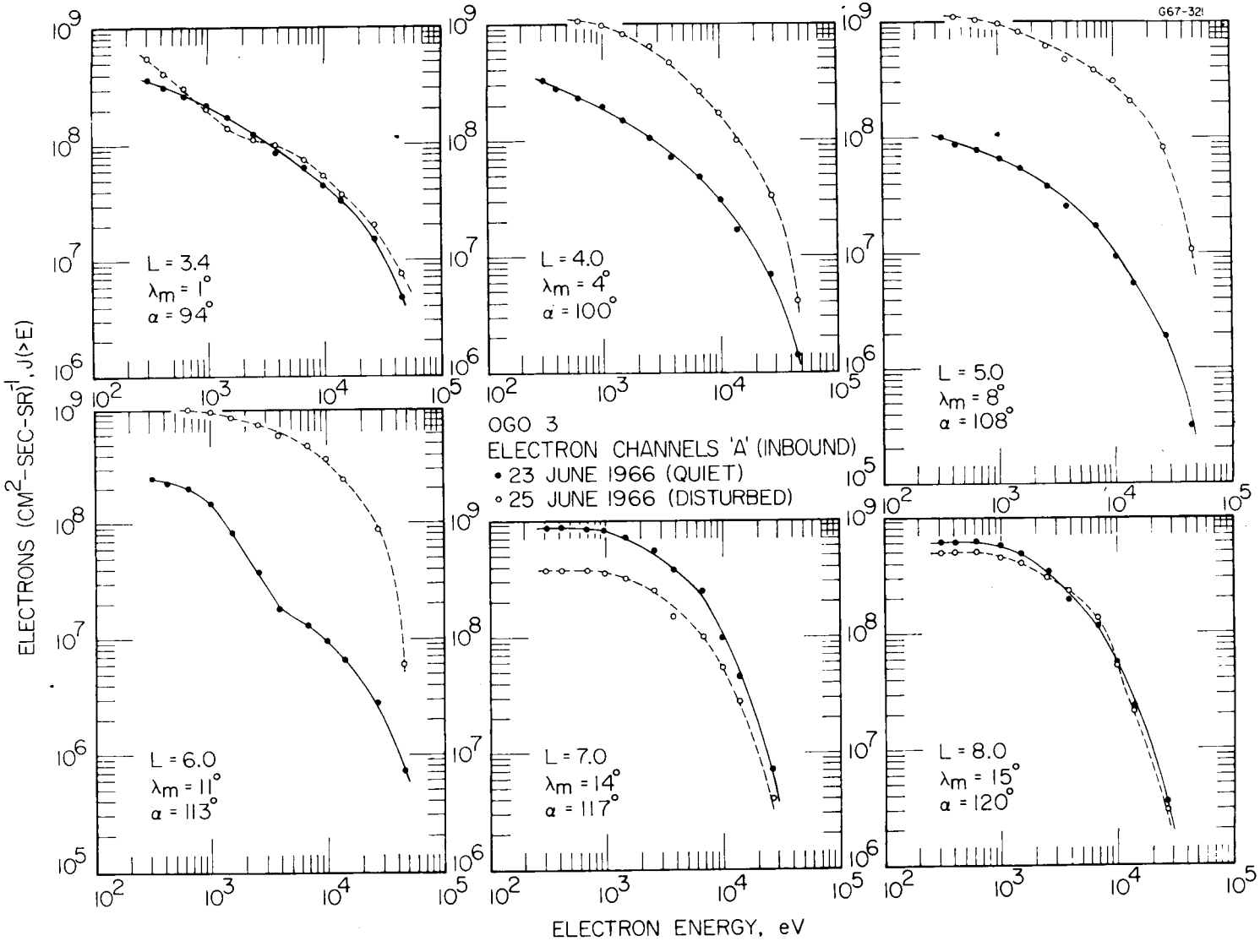
G67-321
L = 3.4
λm = 1°
α = 94°
L = 4.0
λm = 4°
α = 100°
L = 5.0
λm = 8°
α = 108°
L = 6.0
λm = 11°
α = 113°
L = 7.0
λm = 14°
α = 117°
L = 8.0
λm = 15°
α = 120°
OGO 3
ELECTRON CHANNELS 'A' (INBOUND)
• 23 JUNE 1966 (QUIET)
∘ 25 JUNE 1966 (DISTURBED)
ELECTRONS (CM²-SEC-SR)⁻¹, J(>E)
ELECTRON ENERGY, eV

Figure 15

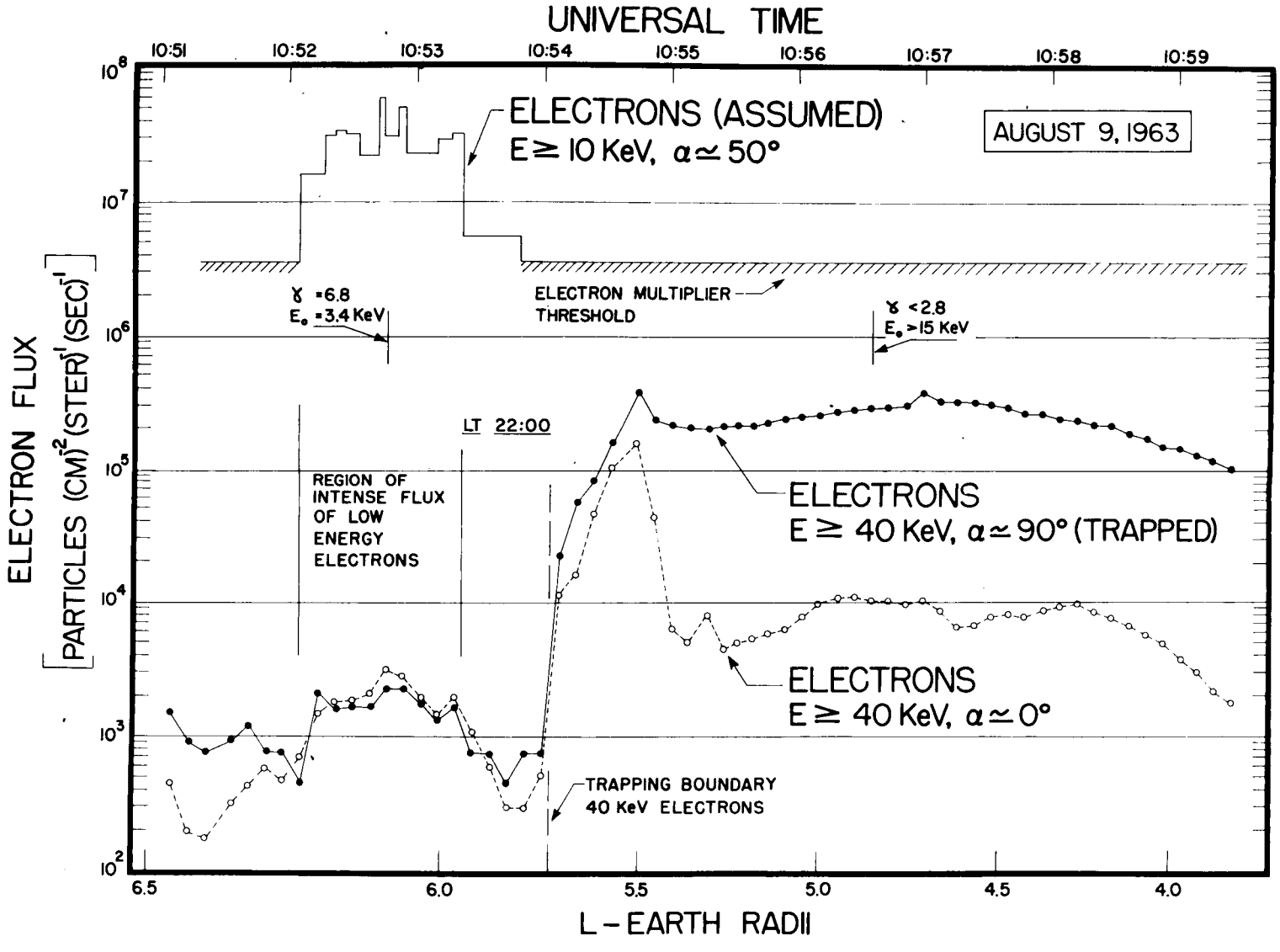
UNIVERSAL TIME
10:51
10:52
10:53
10:54
10:55
10:56
10:57
10:58
10:59
ELECTRONS (ASSUMED)
E ≥ 10 KeV, α ≃ 50°
AUGUST 9, 1963
ELECTRON MULTIPLIER
THRESHOLD
γ =6.8
E₀ =3.4 KeV
γ <2.8
E₀ >15 KeV
LT 22:00
REGION OF
INTENSE FLUX
OF LOW
ENERGY
ELECTRONS
ELECTRONS
E ≥ 40 KeV, α ≃ 90° (TRAPPED)
ELECTRONS
E ≥ 40 KeV, α ≃ 0°
TRAPPING BOUNDARY
40 KeV ELECTRONS
ELECTRON FLUX
[PARTICLES (CM)⁻²(STER)⁻¹(SEC)⁻¹]
10⁸
10⁷
10⁶
10⁵
10⁴
10³
10²
6.5
6.0
5.5
5.0
4.5
4.0
L - EARTH RADII

Figure 16

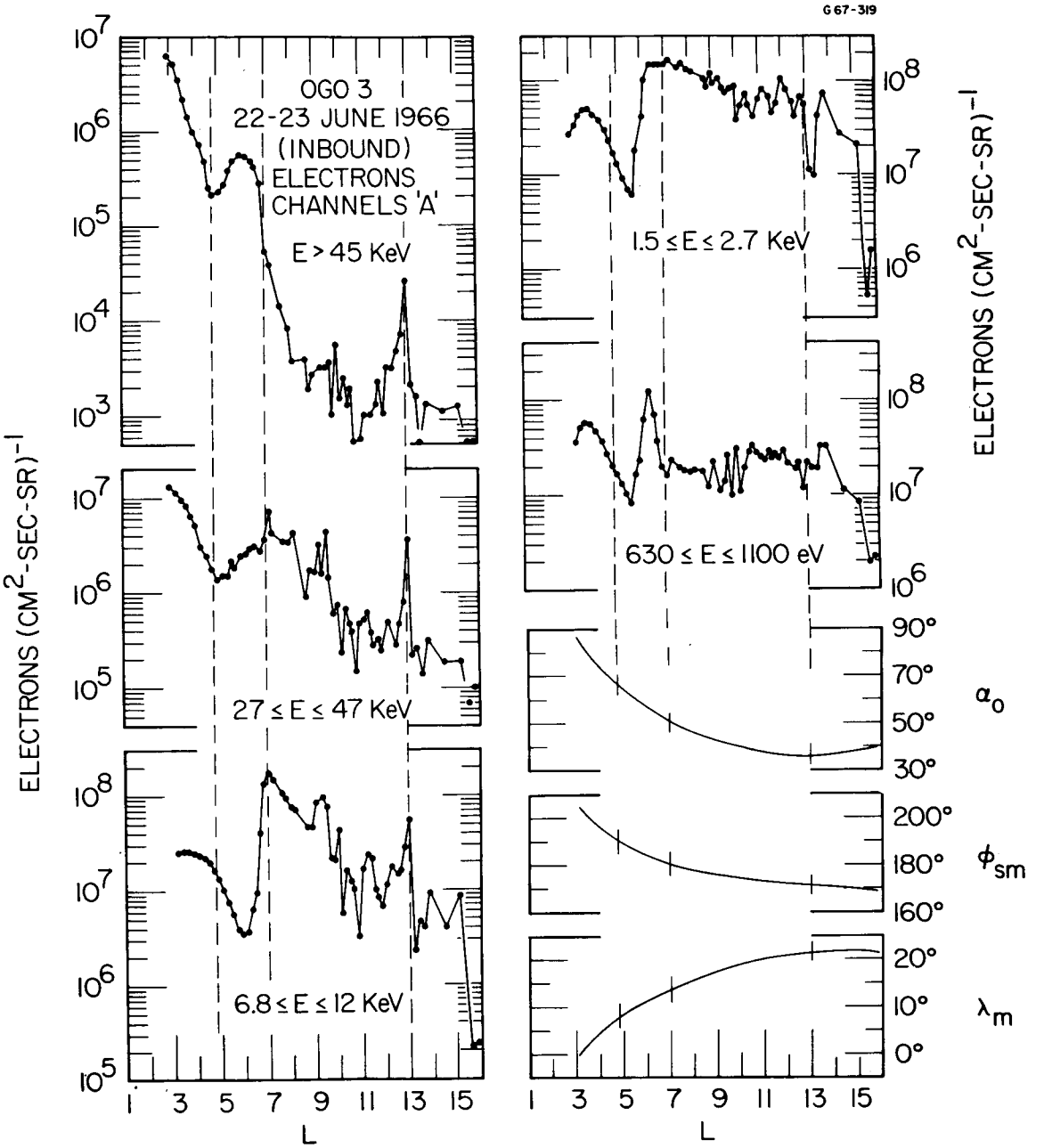
G67-319
OGO 3
22-23 JUNE 1966
(INBOUND)
ELECTRONS
CHANNELS 'A'
E > 45 KeV
27 ≤ E ≤ 47 KeV
6.8 ≤ E ≤ 12 KeV
1.5 ≤ E ≤ 2.7 KeV
630 ≤ E ≤ 1100 eV
ELECTRONS (CM²-SEC-SR)⁻¹
L
α_o
ϕ_{sm}
λ_m

Figure 17

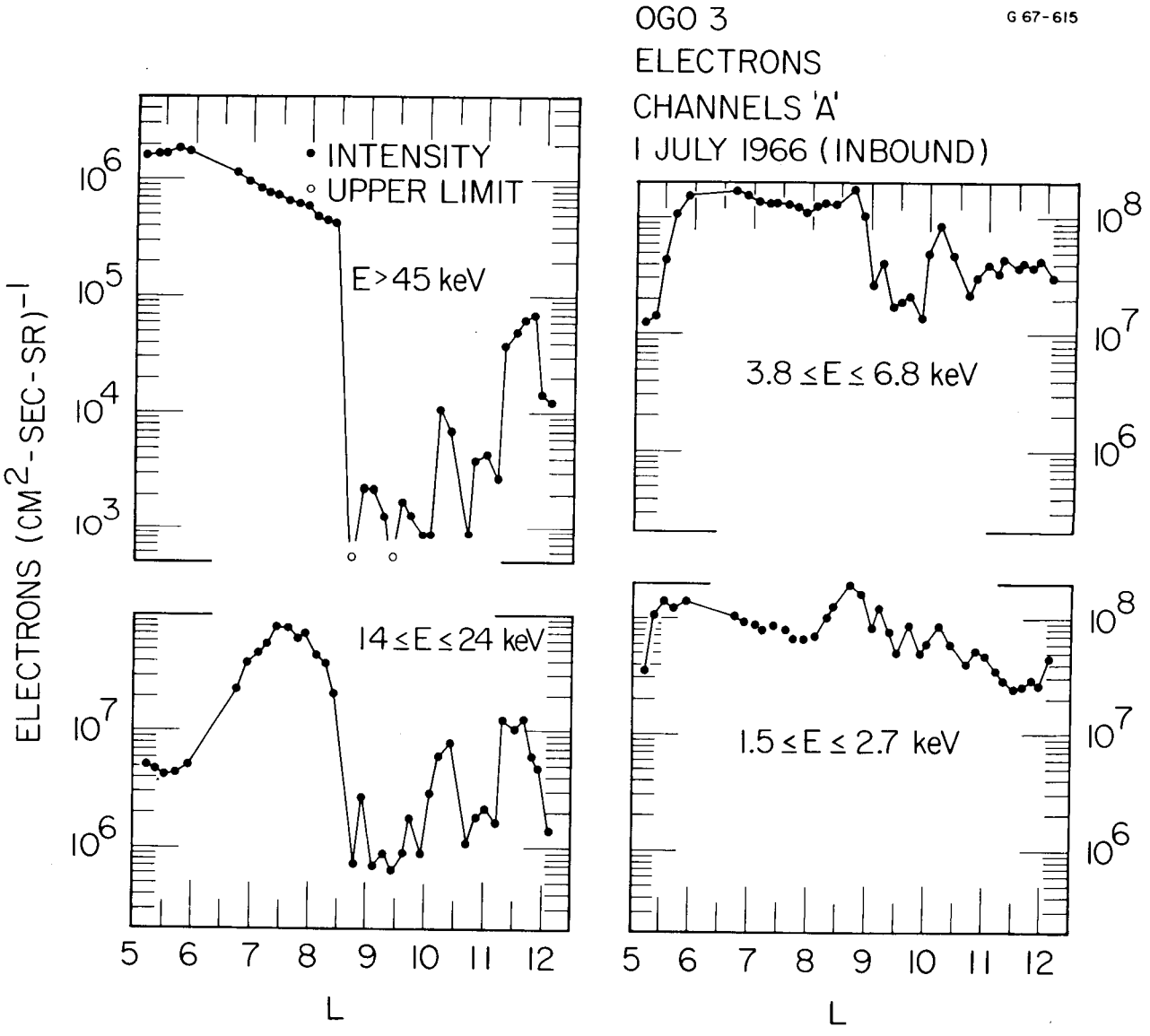
OGO 3
G 67-615
ELECTRONS
CHANNELS 'A'
1 JULY 1966 (INBOUND)
• INTENSITY
◦ UPPER LIMIT
E>45 keV
3.8 ≤ E ≤ 6.8 keV
14 ≤ E ≤ 24 keV
1.5 ≤ E ≤ 2.7 keV
ELECTRONS (CM2-SEC-SR)-1
L
L

Figure 18